

Universidade do Minho
Escola de Engenharia

Ana Cristina Oliveira Correia

**Shape Memory Chitosan-based Scaffolds
for Biomedical Applications**



Universidade do Minho

Escola de Engenharia

Ana Cristina Oliveira Correia

Shape Memory Chitosan-based Scaffolds for Biomedical Applications

Dissertação de Mestrado
Mestrado Integrado em Engenharia Biomédica
Ramo de Biomateriais, Reabilitação e Biomecânica

Trabalho efetuado sob a orientação do
**Professor Doutor João Filipe Colardelle de
Luz Mano**

outubro de 2013

Nome: Ana Cristina Oliveira Correia

Endereço eletrónico: a55585@alunos.uminho.pt

Número do Bilhete de Identidade: 13727892

Título dissertação: Shape Memory Chitosan-based Scaffolds for Biomedical Applications

Ano de conclusão: 2013

Orientador: Professor Doutor João Filipe Colardelle de Luz Mano

Designação do Mestrado: Mestrado Integrado em Engenharia Biomédica

Ramo: Biomateriais, Reabilitação e Biomecânica

É AUTORIZADA A REPRODUÇÃO PARCIAL DESTA TESE/TRABALHO,
APENAS PARA EFEITOS DE INVESTIGAÇÃO, MEDIANTE DECLARAÇÃO
ESCRITA DO INTERESSADO, QUE A TAL SE COMPROMETE.

Guimarães, ____/____/____

Assinatura: _____

Acknowledgments

This work represents the end of my academic journey. And finally, its time to express my sincere thanks to all of those that somehow have contributed throughout this journey, especially in this thesis.

I would like to acknowledgments my supervisor, Prof. João Mano, for all the support, advices, availability and opportunities given. For all the ideas that pushed me further every day. I couldn't reach these results without his guidance.

I would also like to thank Álvaro for the patience, the guidance, the availability and principally for the daily teaching. For all the talks and confidences, for always being ready to help. You became a good friend.

To Ana Rita Duarte, for the guidance, for all the help during this project and for the patient and availability to explain all my doubts. For giving me strength and encouragement.

I want also thank Joana Marques Silva and Sofia Caridade, for the endless hours spent in the DMA experiments. Thanks Joana for always being ready to help and for your contagious joy, sorry for the back pain from the DMA.

To all researchers and staff of 3B's I would like to thanks the good environment and help they provided throughout this work.

I wish to thank Prof. Pamela Habibovic for welcoming me so well in the Department of Tissue Regeneration at University of Twente during my academic Erasmus period. To David for guiding me during my first steps in the lab and for transmitting me all is passion about science. To all my friends that shared with me those six months. It was an experience that I will never forget.

To my friends that start this journey with me, and since the beginning walked by my side. I don't have words to say how much grateful I am for having you as my partners during this journey. You turn these five years the best years of life and I couldn't have done without you. But I know that this is only the beginning. We became a family since 2008 and families are forever, no matter what happens. I love you all!

To my two little kids, that are so grown. Now that it's tome for me to leave I think you don't need my guidance anymore. I am so proud of you and of what you become. Thanks for choosing me!

To the friends I made in the Student's Union and for all the experiences they share with me. I will never forget all the time we spend together and how much I learned and growth during this experience. Thank you for making me part of it. Thank for you friendship.

I want also thank to my oldest friends, that are with me since ever. I thank them with all my heart. They were extremely important to me during my live and during this journey. For all the emotional support, understanding, affection, and constant encouragement, I am deeply grateful. The knowledge that they will always be there to pick me up, helping me and making me smile is what allowed me to keep on moving even in difficult times. They believe in me more that I did.

Taipas, I can't imagine this journey without you. For all the experiences we shared together, for all the advices, talks, laughs and cries and for all the crazy ideas that no one else would understand. To making everything simple and for read me with just one look. For TT house, Erasmus and all the experiences, I can say that you are the best bad influence ever! Looking at all we went through, I know that despite of what happens you are my best friend, which I will always keep next to me.

To Luis, you know how important you are to me.

To all my family: my uncles, my aunts and my cousins. Thank you for helping me whenever I needed, for being my friends and for believing in me. A special thanks to my cousins, Ana and Raquel, and my aunt Tia Rucas that were always so enthusiastic about my academic course and always believe that I will have a brilliant future.

To my brother and to my parents. For all the support, encouragement and for always believed in me. For supporting me in every decision and for always picked me up whenever I felt down. Thank you so much for everything you have done for me. I don't have words to describe how grateful I am.

Abstract

The searching for materials that display mechanical properties able to satisfy the specifications required by their implantation aroused a great interest in the context of shape memory materials. Shape memory polymers (SMPs) offer novel materials-based devices to solving scientific challenges due to their demonstrated ability to actively undergo geometric transformations upon exposure to environmental stimuli. The most attractive SMPs are still thermal-induced SMPs due to their wide availability and broad possible applications. However, shape memory triggered by temperature is not the best control method for applications taking place within narrow temperature ranges, which is the case of biomedical applications.

In this work we hypothesize that we could develop new devices in which the recovery of the geometry can be induced by hydration. Non-crosslinked and genipin-crosslinked chitosan scaffolds, showing a shape memory effect are presented and characterized in this work. The developed scaffolds can be rapidly expanded from a compressive state to its expanded state, stimulated by hydration in an aqueous environment, during which the glass transition takes place and the chain segmental mobility permits the recovery of the permanent shape of the device. For the proof of concept, the shape memory effect of chitosan was followed by compressive tests to measure the shape memory parameters: shape fixity and shape recovery. Mechanical properties were also studied by dynamic mechanical analysis (DMA), while the sample was immersed in gradient compositions of water/ethanol mixtures. Moreover we also analyze if the scaffolds could present multifunctional properties that ally shape memory with drug release. For that, *in vitro* drug delivery studies were performed.

The chitosan scaffolds were also reinforced with bioactive glass nanoparticles in order to produce porous nanocomposites that combine the shape memory properties of chitosan and the apatite deposition ability of the nanoparticles. These scaffolds were characterized by the same compressive test performed with the chitosan scaffolds and by *in vitro* bioactivity tests.

The scaffolds developed in this work show a shape memory behavior induced by hydration with good shape memory properties that can be used as systems for applications in minimally invasive surgery or drug delivery with a good ability to geometrically accommodate to bone defects upon implantation. Moreover, the chitosan scaffolds containing bioactive glass nanoparticles showed, aside the good shape memory properties obtained by the chitosan, a bioactivity character induced by the nanoparticles. Thereby, we consider that these scaffolds have potential as shape-memory implants for bone regeneration.

Resumo

A procura de materiais que desempenhem propriedades mecânicas capazes de satisfazer as especificações exigidas para implantação despertou um grande interesse em materiais com memória de forma. Dispositivos baseados em polímeros com memória de forma (SMPs) oferecem soluções capazes de resolver desafios científicos complexos, devido à habilidade de alterar a sua forma quando estimulados por agentes externos. Dentro dos SMPs, os polímeros mais utilizados são os SMPs que respondem a estímulos térmicos, devido à sua ampla disponibilidade e ao elevado número de aplicações. No entanto, SMP estimulados por temperatura não são o melhor método para aplicações limitadas a uma baixa gama de temperaturas, como é o caso de aplicações biomédicas.

Neste trabalho testamos a hipótese de conseguir desenvolver novos dispositivos que sejam capazes de recuperar a sua forma inicial induzidos por hidratação. "Scaffolds" de quitosano não reticulados e reticulados com genipin que mostram efeito de memória de forma são apresentados e caracterizados neste trabalho. Para provar esta característica dos "scaffolds", o efeito de memória de forma do quitosano foi analisado através de testes de compressão para medir os parâmetros de memória de forma: capacidade de fixar a forma temporária e capacidade de recuperar a forma inicial. As propriedades mecânicas foram também avaliadas usando análise dinâmica mecânica (DMA), enquanto as amostras estavam imersas em soluções de água/etanol com diferentes gradientes. Além disso também foi analisado se os "scaffolds" apresentam propriedades multifuncionais que aliam memória de forma com libertação controlada de fármacos. Posteriormente, os "scaffolds" de quitosano foram reforçados com nanopartículas de vidro bioactivo de forma a produzir um nano-compósito, que combine as propriedades de memória de forma do quitosano e a mineralização induzida pelo "biovidro", para aplicações de Engenharia de Tecidos aplicada ao osso.

Os "scaffolds" desenvolvidos mostram um comportamento de memória de forma induzida por hidratação com boas propriedades de memória de forma que podem ser usados como sistema de libertação controlada de fármacos para aplicações em cirurgias não invasivas ou para libertação de fármacos. Além disso, os "scaffolds" de quitosano combinados com as nano-partículas de biovidro mostram boas propriedades de memória de forma, devido ao quitosano, e um carácter bioactivo induzido pelas nano-partículas. Deste modo, estes "scaffolds" têm potencial como um implante para regeneração óssea.

Table of Contents

Acknowledgments.....	III
Abstract.....	V
Resumo.....	VII
Table of Contents	IX
List of abbreviations.....	XIII
List of Figures	XV
List of Tables.....	XIX

Chapter I. - General Introduction 1

1. Motivation and Outlines.....	3
2. Shape memory polymers.....	4
2.1 Molecular structure of shape memory polymers.....	5
3. Thermomechanical cycle.....	8
4. Dual and triple-shape memory effect.....	9
5. Trigger mechanisms	11
5.1 Water-responsive SMP.....	12
6. Polymeric material with shape memory behavior.....	13
6.1 Chitosan.....	14
6.2 SMP Composites.....	16
6.2.1. Bioactive Glass Nanoparticles (BG-NPs)	17
7. Biomedical Applications of SMPs	18
7.1 Drug delivery Systems	19
8. Conclusions and Outlook.....	20
9. References.....	20

Chapter II. - Materials and Methods..... 27

1. Materials.....	29
2. Methods.....	29
2.1 Chitosan Purification.....	29
2.2 Chitosan scaffolds preparation.....	29

2.3 Genipin-crosslinked Chitosan Scaffolds	30
2.4 Bioglass nanoparticles (BG-NPs) preparation	30
2.5 Chitosan/BG-NPs Scaffolds preparation.....	31
2.6 Scanning Electron Microscopy (SEM).....	31
2.7 Porosity measurements.....	31
2.8 Energy Dispersive Spectroscopy (EDS).....	31
2.9 Fourier Transform Infrared Spectroscopy (FTIR).....	32
2.10 Swelling Properties	32
2.11 Hydromechanical Cyclic Compression Tests.....	33
2.11.1 Recovery vs time	35
2.12 Dynamic Mechanical Analysis (DMA).....	35
2.13 X-ray diffraction measurements.....	36
2.14 <i>In vitro</i> drug delivery studies	36
2.15 <i>In vitro</i> bioactivity study	38
2.16 Micro-Computed Tomography (μ -CT).....	38
3. References	39

Chapter III. - Chitosan Scaffolds with Shape Memory induced by Hydration..... 41

1. Introduction	44
2. Materials and Methods	46
2.1 Materials.....	46
2.2 Methods.....	46
2.2.1 Chitosan Scaffolds Preparation	46
2.2.2 Scanning electron microscopy (SEM).....	46
2.2.3 Porosity measurements.....	46
2.2.4 Swelling of chitosan scaffolds in water/ethanol mixtures.....	47
2.2.5 X-ray diffraction measurements	47
2.2.6 Dynamic Mechanical Analysis (DMA).....	47
2.2.7 Hydromechanical Cyclic Compressive Tests.....	48
2.2.8 <i>In vitro</i> drug delivery studies	49
3. Results and Discussion.....	50
3.1 Morphological Characterization.....	50
3.2 Swelling of chitosan scaffolds in water/ethanol mixtures.....	51
3.3 Dynamical mechanical analysis measurements	53
3.4 Shape memory behavior of chitosan	55
3.5 Young's modulus of the scaffolds at distinct hydration levels	57

3.6 Hydromechanical compressive cycle	58
3.7 <i>In vitro</i> drug delivery studies	59
4. Conclusions	61
5. Acknowledgments	61
6. References	61

Chapter IV. - Chitosan/Bioactive Glass Nanoparticles Scaffolds with Shape Memory Properties..... 65

Abstract	67
1. Introduction	68
2. Materials and Methods	69
2.1 Materials	69
2.2 Methods	69
2.2.1 Bioglass nanoparticles (BG-NPs) preparation	69
2.2.2 Scaffolds Preparation	70
2.2.3 <i>In vitro</i> bioactivity study	70
2.2.4 Scanning Electron Microscopy (SEM) and Energy Dispersive Spectroscopy (EDS)	71
2.2.5 Fourier-Transformed Infrared (FTIR) spectroscopy analysis	71
2.2.6 Swelling of scaffolds in water/ethanol mixtures	71
2.2.7 Hydromechanical Cyclic Compressive Tests	71
2.2.8 Micro-Computed Tomography (μ -CT)	72
3. Results and Discussion.....	73
3.1 Bioactivity study	73
3.2 Swelling of CHT and CHT/BG-NPs scaffolds in water/ethanol mixtures	75
3.3 Mechanical Properties	76
3.3.1 Young's modulus of the scaffolds at distinct hydration levels	77
3.3.2 Hydromechanical compressive cyclic	78
4. Conclusion.....	81
5. Acknowledgments	82
6. References	82

Chapter V. - General Conclusions and Future Perspectives..... 85

List of abbreviations

B		G	
β	Beta	g	Gram
BG-NPs	Bioglass Nanoparticles;	GPa	GigaPascal
C		H	
Ca	Calcium	h	Hours
CHT	Chitosan	Hz	Hertz
CHT0	Non-crosslinked CHT scaffold		
CHT1	Crosslinked CHT scaffold	I	
CHT/B G-NPs	Chitosan with bioglass nanoparticles scaffold	IE	Incorporation Efficiency
cm	Centimeters	K	
CR	Congo Red	KBr	Potassium Bromide
D		kDa	Kilodaltons
DD	Degree of Deacetylation	M	
DMA	Dynamic Mechanical Analysis	MPa	MegaPascal
E		μm	Micrometers
ϵ_m	Maximum strain	mA	Miliamperes
ϵ_p	Permanent strain after recovery	ml	Milimeters
ϵ_u	Temporary shape strain	mm	Milimeters
E	Young's Modulus	min	Minutes
E'	Storage Modulus	M	Molar
ECM	Extracellular Matrix	N	
EDS	Energy Dispersive Spectroscopy	N	Number of cycle
Eq	Equations	NaOH	Sodium Hydroxide
F		nm	Nanometers
FTIR	Fourier Transform Infrared		

P	Spectroscopy	T	
P		θ	Theta
PBS	Phosphate	$\tan \delta$	Loss factor
PCL	Phosphate Buffered Saline	TE	Tissue Engineering
PEG	Polycaprolactone	Tg	Glass Transition
PGA	Polyethyleneglycol	Tm	Melting Temperature
PLA	Polyglycolide		
PMA	Poly(lacticacid)	U	
Q	PMMA	UV	Ultraviolet
	PU		
	Polyurethane	V	
R		v/v	Volume/volume
	Q	Veth	Volume of etanol
	Caudal		
S		W	
	R_f	w	Weight of the swollen scaffold
	R_r	w/v	Weight/volume
	Strain Fixity Rate	w_0	Weight of the dry scaffold
	Strain Recovery Rate		
	SBF	X	
	SEM	XRD	X-Ray Diffraction
	SM		
	SMA		
	SME		
	SMP		
	SMPU		
	Shape Memory Polymers		
	Shape Memory Polyurethane		

List of Figures

Chapter I. - General Introduction

- Figure I.1** Schematic representation of the shape memory effect (Adapted from ³⁴).
- Figure I.2** Schematics of the typical structures of a polymer network that is (a) physically crosslinked network; (b) chemically ³⁷.
- Figure I.3** Molecular mechanism of the thermally induced shape-memory effect (T_{trans} = thermal transition temperature related to the switching phase) ³⁵.
- Figure I.4** Variations of SMP's elastic modulus with temperature.
- Figure I.5** Stress-strain-temperature cycle for a thermoplastic shape-memory polymer with a thermally induced shape memory effect ³⁴.
- Figure I.6** Triple-shape effect of polymer network ⁴⁶.
- Figure I.7** Chemical structure of chitin and chitosan ⁹⁴.

Chapter II. - Materials and Methods

- Figure II.1** Schematic of the programming and recovery process of the SME.
- Figure II.2** Calibration Curve of Absorbance of Congo Red.

Chapter III. - Chitosan Scaffolds with Shape Memory induced by Hydration

- Figure III.1** SEM images of porous non-crosslinked (CHT0) and crosslinked (CHT1) chitosan scaffolds.

-
- Figure III.2** Swelling capability of non-crosslinked (CHT0) and crosslinked (CHT1) chitosan scaffolds determined after immersion in distinct water/ethanol mixtures.
- Figure III.3** XRD pattern for CHT0 immersed in different mixtures of water/ethanol from 0% to 100% of water.
- Figure III.4** Apparent storage modulus (A) and loss factor (B) measured with samples immersed in water/ethanol mixtures for CHT0 and CHT1 at 1Hz.
- Figure III.5** CHT0 shape recovery along time after different maximum strains (ϵ_m) (A). Series of photographs demonstrating the shape recovery process for CHT0; the refereed times indicate the immersion time in water upon deformation at $\epsilon_m=30\%$ and dehydration (B).
- Figure III.6** A - Strain recovery of CHT0 in different mixtures of water/ethanol after different ϵ_m . B - Strain recovery of CHT0 and CHT1 for $\epsilon_m=30\%$.
- Figure III.7** The variation of Young's Modulus with water/ethanol mixtures for CHT0 and CHT1.
- Figure III.8** Hydromechanical compressive cycle of CHT and CHT/BG-NPs. I: compression at a constant rate of the hydrated sample; II - dehydration of the sample at a fixed strain; III - release of the stress; IV - hydration in water/ethanol mixtures with increase content in water.
- Figure III.9** A - *In vitro* release of CR as a function of time for CHT0 and CHT1 in PBS (37°C). B - Images showing CR being release from a CHT0 scaffold after being placed in a defect produced in a gelatin block.

Chapter IV. - Chitosan/Bioactive Glass Nanoparticles Scaffolds with Shape Memory Properties

- Figure IV.1** SEM micrographs of CHT/BG-NPs soaked in the SBF solution during 0 (A), 3 (B) and 7 (C) days and the corresponding characterization of the chemical elements using EDS.
- Figure IV.2** FTIR spectra of the powders scratched from the surface of the patterned membranes after 0 (control) and 7 days of immersion in SBF.
- Figure IV.3** Dependence on the swelling capability of CHT and CHT/BG-NPs scaffolds determined after immersion in water/ethanol mixtures.
- Figure IV.4** The variation of Young's Modulus with water/ethanol mixtures for CHT and CHT/BG-NPs.
- Figure IV.5** Hydromechanical compressive cycle of CHT and CHT/BG-NPs. I: compression at a constant rate of the hydrated sample; II - dehydration of the sample at a fixed strain; III - release of the stress; IV - hydration in water/ethanol mixtures with increase content in water.
- Figure IV.6** Strain recovery of CHT and CHT/BG-NPs in different mixtures of water/ethanol for $\epsilon_m=30\%$.
- Figure IV.7** A- Illustration of CHT/BG-NPs recovery in a defect produced in a pig femur bone. B - Representative images of tree orthogonal Micro CT slices of a CHT/BG-NPs scaffold after recovery in the bone defect.

List of Tables

Chapter II. - Materials and Methods

Table II.1 Comparison between ion concentration in SBF and in human blood plasma.

Chapter III. - Chitosan Scaffolds with Shape Memory induced by Hydration

Table III.1 Shape memory properties of CHT0 and CHT1 at different deformation strains (ϵ_m).

Chapter I. - General Introduction

1. Motivation and Outlines

Tissue engineering (TE) has the aim to repair human tissue that has been aged, damaged or lost from injury, disease or infection so that its initial functions are restored. TE strategies may combine materials and cells, relying on the advancement in the engineering of innovative bioactive and biodegradable materials to make use of the body's natural repair mechanisms¹. In general, materials for TE should encourage tissue regeneration by favorably reacting with surrounding living tissues when exposed to physiological fluids^{2,3}. Simultaneously, biomaterials used for TE can present other properties that can be useful for the handling and the implantation protocol.

Motivated by the increasing need for custom-made materials for specific medical applications, researchers have progressively begun an interdisciplinary work in the hopes of creating high-performance biomaterials with specific properties into high-potential biomaterials candidates^{4,5}. Polymeric biomaterials are presently applied in many biomedical applications such as implants, surgical instruments, wound covers and controlled drug-delivery systems⁶⁻⁸. Each application requires a specific combination of material properties and functions.

The rapid progress in the development of surgical techniques, especially in minimally invasive surgery, leads to more complex requirements for modern implants. Aside the important properties like biocompatible and, ideally in many cases, degradability, the shape memory effect (SME) as a novel functionality of polymers might enable the development of novel types of medical devices⁹⁻¹¹. Shape memory polymers (SMPs) offer novel materials-based devices to solving scientific challenges due to their demonstrated ability to actively undergo geometric transformations upon exposure to environmental stimuli^{8,12}.

The goal of this work is to develop chitosan scaffolds with shape memory properties. It was found before that Chitosan can undergo a glass transition by the action of hydration^{13,14}. By combining such effect with the maintenance of the structural

integrity of the system (provided by crosslinking or due to the semi-crystalline structure) we hypothesize that we could develop new devices in which the recovery of the geometry can be induced by hydration. The porous structure was chosen based on the fact that porous shape memory polymeric materials possess certain material capabilities such as greater volumetric expansion with high surface area that allow ingrowths of cells and act as a physical support to guide the differentiation and proliferation of cells into the target functional tissue or organ ^{15,16}.

2. Shape memory polymers

Shape memory polymers (SMPs) represent a technologically important class of stimuli-responsive materials for which the response lies in the shape change, being defined as "adaptive" or "smart" materials ¹⁷. Smart or adaptive are adjectives given to those materials that provide a specific response in a particular environment ^{18,19}. More specifically, the conventional definition of an SMP is a polymer can be deformed and subsequently fixed into a temporary shape, which would remain stable unless it is exposed to an appropriate external stimulus that triggers the polymer to recover its original (or permanent) shape ²⁰.

The first recorded observation of the shape memory transformation was discovery in gold alloys by Chang and Read in 1932 ²¹ and since that, the SME has been extensively investigated in metal alloys for its potential use in medicine ^{4,22}. The development of SMP began years later, with polyethylene as heat-shrinkable material in 1960 ²³. However, the first time that was used the SMP term started with the development of SMP polynorbornene by CDF Chimie Company (France) in 1984 ¹⁸.

Shape memory materials, in particular shape memory alloys (SMAs), have been used in a wide range of engineering applications for many years ^{24,25}. More recently, SMPs have been attracting a lot of attention due to their great potential, in particular for biomedical applications ²⁶.

SMP have many advantages compared to metallic shape memory alloys. SMAs present difficulties on fabrication, high cost and limited recoverable deformation. SMAs are only able to recover from deformations up to 10%, above which plastic deformation with unrecoverable shape change can occur ^{18,27}. On the other hand, SMPs have an easier availability, are cheaper, light weight, and have a wide range of mechanical and physical properties. They can recover from deformations well over 100% and can go

through a high number of repetitions without any significant material degradation ^{27,28}.

For biomedical applications they can also present advantages such as biocompatibility, nontoxicity and biodegradability ^{5,29}. This has triggered an interest in polymers with high specific shape memory characteristics that represented a cheaper and more efficient alternative to established SMAs.

A shape-memory polymer can be deformed by application of an external stress and fixed in a second shape, the temporary shape. This temporary shape is retained until the shaped body is exposed to an appropriate stimulus, which induces the recovery of the original shape. The movement during recovery from the temporary shape to the original shape reverses the mechanical deformation ⁸.

Shape memory research was first built on the thermally-induced shape memory effect, where the heat is the direct stimulus to the shape change ¹¹. However, depending on the polymer structure or additional components (in the case of composites), shape memory effect can also be triggered by diverse stimuli ranging from light ³⁰, electrical ³¹, magnetic stimulation ³² or hydration ³³.

2.1 Molecular structure of shape memory polymers

The shape memory effect (SME) results from a combination of molecular polymer network architecture and a specific processing and programming technology. In general terms, SME requires three stages: processing, programming, and recovery (Figure I.1). The polymer is processed into its initial shape, the permanent shape. By programming, the polymer is deformed into the temporary, fixed shape by the effect of an external action; this process is also named as a "shape-memory creation process". Finally, by the application of the appropriate external stimulus, the polymer recovers its original and permanent shape. This cycle of programming and recovery can be repeated several times, with different temporary shapes in subsequent cycles ^{34,35}.

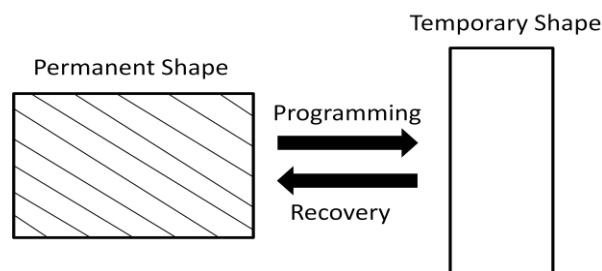


Figure I.1 - Schematic representation of the shape memory effect (Adapted from ³⁴).

SMP contain a network architecture consisting of netpoints that are connected with stimuli-sensitive macromolecular chains. The netpoints, which are connected by chain segments, determine the permanent shape and the chain segments are using as a kind of molecular switch. The network architectures are constructed through crosslinking netpoints, with polymer segments connecting adjacent netpoints. These strongly crosslinked architectures ensure that the polymer can maintain a stable shape on the macroscopic level for enabling both the original and recovered shapes¹⁸. The network that sets the permanent shape can be of chemical nature (covalent bonds) or of physical nature (intermolecular interactions) (Figure I.2). Physical crosslinking is obtained in a polymer, whose morphology consists of at least two segregated domain, the network is achieved by the formation of crystalline or glassy phases. Physically crosslinked polymers (thermoplastics) exhibit a reversible nature. For the chemically crosslinked polymers (thermosets), the individual polymer chains are connected by covalent bonds, which are more stable than the physical crosslinking network and show an irreversible nature^{36,37}. Crosslinking of either chemical or physical nature is responsible for controlling the shape transitions in these materials³⁸.

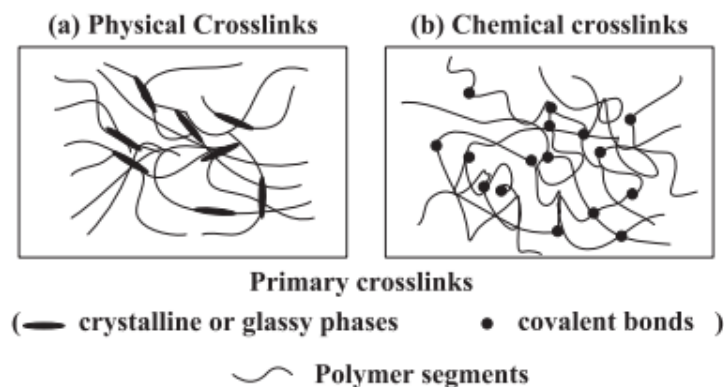


Figure I.2 - Schematics of the typical structures of a polymer network that is (a) physically crosslinked network; (b) chemically³⁷.

The chain segments must allow long range conformational mobility in order to obtain deformation when an external stress is applied, which increases with the increasing of the length and flexibility of these segments. During the programming process that changes the permanent shape into the temporary shape the chain segments are flexible allowing the shape change. A change in some external variable can maintain stable the deformed shape (temporary shape). The recovery from the temporary to the permanent shape is enabled due to the retreating of the chain segments by the reversible

action of the external variable (Figure I.3). The temperature is the most used stimuli to generate the temporary shape and recover the permanent geometry ^{17,34}.

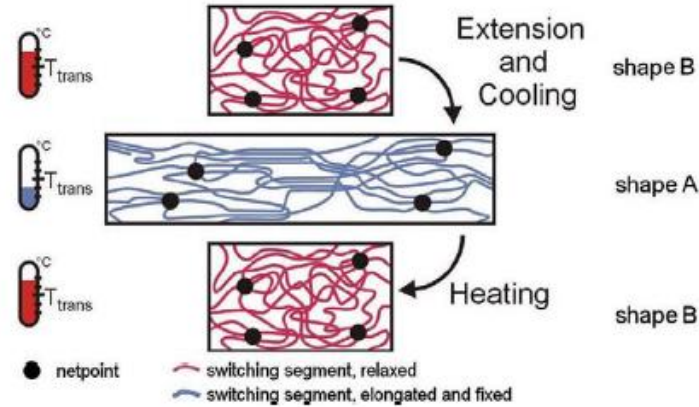


Figure I.3 - Molecular mechanism of the thermally induced shape-memory effect (T_{trans} = thermal transition temperature related to the switching phase) ³⁵.

Temperature shape memory polymers are characterized by having a transition temperature, which is responsible for the change in the network polymer, leading to the shape memory effect. The transition temperature for the fixation of the switching segments can either be glass transition (T_g) or melting temperature (T_m). Glass transitions occur over a large temperature interval, whereas melting temperature occurs over a smaller temperature range ^{37,39}. Besides the temperature, the shape memory technologies can also use other stimulus, such as hydration, light, electromagnetic or electrical to heat the material indirectly.

In thermally induced shape memory polymers at temperatures higher than the T_g , the polymers chain segments are relaxed and flexible. When an external stress is applied, the polymers chain segments are elongated and the netpoints are displaced. Below transition temperature, occurs a freezing of the molecular chain segments, resulting in a shape fixation. Upon reheating above T_g under a stress free condition, the molecular mobility is re-activated, which allows the chains to return the original shape ³⁴.

Figure I.4 illustrates the transition from rubber-elastic state to the glassy state. Above the transition temperature, the polymers are in their rubbery state, elastic and flexible, the stiffness of the polymer is low. The polymer network exhibit "superelasticity". Below the transition temperature the rubbery state is replace for the

glassy state and the polymer become hard and crumbly. Across the T_g is possible to observe changes in the associated elastic modulus. In the case of a transition from the rubber-elastic to the glassy state, the elastic modulus increases and the flexibility of the entire segment is limited. If the polymer is crosslinked or sustained by crystallized domains the elastic deformation induced at high temperature can be kept below T_g . By heating above T_g the chains recover the initial highest entropy state ^{4,27,40}.

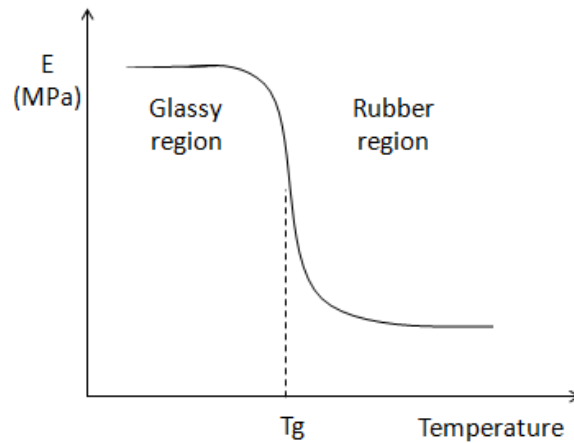


Figure I.4 - Variations of SMP's elastic modulus with temperature.

3. Thermomechanical cycle

The shape memory effect can be represented by a thermomechanical cycle. The process across the changing between the permanent, temporary and permanent shape can be divided in 4 steps: loading, cooling, unloading and recovery. During these steps the temperature and stress-strain response are considered ⁴¹. The procedure can be presented as a two or three dimensional plot, like the one shown in Figure I.5.

In step 1, the sample is loaded to the maximum strain (ϵ_m) at constant temperature, higher than its T_g . This step corresponds to a standard stress-strain test. In step 2, the load is held and the sample is cooled down below T_g under constant strain (ϵ_m), fixing the temporary shape. Step 3 is an unloading step, the strain is reduced until a stress-free condition is achieved at 0 MPa. Finally, in step 4 the sample is heated, while the tensile stress is led constant at 0 MPa, resulting in a recovery of the permanent shape. There is a drastic strain change around the T_g as the temperature passes through this region, as a result of a transition from a glassy state to a rubbery state. Finally, the sample stabilizes at a strain near the starting strain value ^{34,42}.

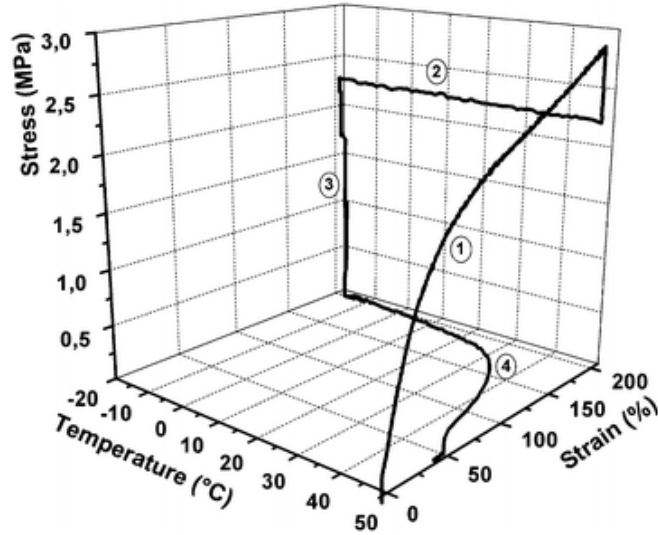


Figure I.5 - Stress-strain-temperature cycle for a thermoplastic shape-memory polymer with a thermally induced shape memory effect ³⁴.

In these cycle tests, the strain fixity rate (R_f) and the strain recovery rate (R_r) are determined ^{18,36,42}. Shape fixity refers to the ability to fix a mechanical deformation, resulting in a temporary shape. Shape fixity can be quantified from the following equation,

$$R_f(N) = \frac{\epsilon_u(N)}{\epsilon_m} \quad (1)$$

where, ϵ_u represents the temporary shape strain and ϵ_m represents the applied maximum strain.

The strain recovery rate quantifies the ability to restore the mechanical deformation of the permanent shape ϵ_p after application of a certain deformation ϵ_m .

For N cycles, the shape recovery is defined as,

$$R_r(N) = \frac{\epsilon_m - \epsilon_p(N)}{\epsilon_m - \epsilon_p(N-1)} \quad (2)$$

where, ϵ_p is the strain associated with the permanent shape.

4. Dual and triple-shape memory effect

Currently known shape memory polymers are capable of memorizing one, two or multiple temporary shapes, corresponding to dual (dual-SME), triple (triple-SME)

and multi-shape memory effects (multi-SME), also counting the permanent shape, respectively^{43,44}.

The most known form of shape memory effect is the dual-SME. A total of two shapes, (one temporary shape and one permanent shape) are involved in each shape memory cycle. Example of dual shape effect was shown before^{18,45}.

The recent emerged triple-SME has a total of three shapes involved and represents more or less an extension of the traditional dual-SME. Generally, a triple-SMP is ascribed to a multiphase polymer network that contains at least two separated domains, which are associated with individual transition temperatures. The polymer with triple-SME has two distinct T_g or T_m in contradiction to the dual-SME that only have one. Relative to the dual-shape cycle which has one shape fixing and one shape recovery step, a triple shape cycle comprises two shape-fixing and two shape recovery step^{43,46,47}.

Figure I.6 shows an example of a triple-SME. The SMP is able to change from a first shape (A) to a second shape (B) and finally deform into a third shape (C). For the first deformation, from the permanent shape (A) to the temporary shape (B), the polymer was deformed by imposing a stress and fixing by cooling to a temperature between the two T_g s. The second temporary shape (C) is derived from imposing a second stress (different from the first) and using a fixation temperature below both T_g s. Shape recovery is conducted under a stress free condition. The recovery from sample C to sample B is achieved by heating the polymer to a temperature between the both T_g s and the recovery from sample B to the permanent shape (A) is obtained by heating to a temperature above both T_g s^{48,49}.

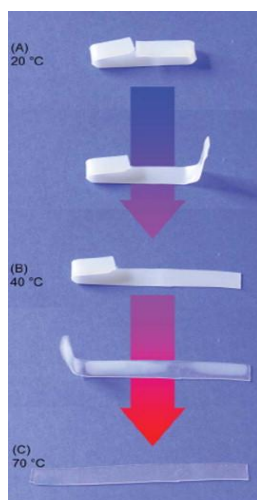


Figure I.6 - Triple-shape effect of polymer network⁴⁶.

Recently has emerged studies in multi SMEs, which can remember more than two temporary shapes ^{44,50}. Xie et al. exploited the new multiple SME systems based on multi composite SMPs made of Fe₃O₄-SMP region and a carbon nanotube region separated by the neat Tg-type SMP region. The multi-composite demonstrated well-controlled multiple shape recoveries ⁵¹. Li et al, created a quintuple-SME using PMMA/PEG systems by utilizing three separated temperatures within the glass transition and additionally T_m of PEG as four transition temperatures. This system can achieve the multiple-SME from dual to quintuple, which can be adjusted by simply choosing the suitable temperatures from the broadened glass transition and T_m ⁵².

The discovery of triple and multi SME will stimulate the development of shape memory functions to fulfill the requirements of increasingly complex applications.

5. Trigger mechanisms

Although direct heat remains the main trigger of shape memory behavior in polymers, such an approach is not always practical. SMP driven by external heat are an issue for applications with restricted temperature ranges like in biomedical field ⁴². Therefore, search has been done for alternative triggering mechanisms. Shape memory can also be light-induced process, electro-active, water/moisture/solvent induced, pH sensitive and magnetic-sensitive, based on their external stimulus ^{19,42}. During the process, the materials are heated directly or indirectly above their glass transition temperature that trigger the shape memory effect ⁵³.

In the present, the most attractive SMPs are still thermal-induced SMPs due to their wide availability and broad possible applications ⁵⁴. However, their triggering conditions or controlling method are not so practical since thermal triggering shape memory is not the best control method in most applications. In the case of applications with temperature limited to a low temperature range like biomedical applications, this can be an issue ^{42,55}. Non-thermally induced shape memory polymers eliminate the temperature constrains and enable the manipulation of the shape recovered under ambient temperature ⁵⁶.

5.1 Water-responsive SMP

Recent studies have shown that the environmental conditions such as the humidity can substantially influence conformational mobility of macromolecular chains, and thus the shape memory properties of polymers⁵⁷⁻⁶¹. These findings motivated the development of the concept of a moisture triggered SME^{62,63}.

Water or solvent-driven shape recovery effects have been observed in SMPs having glass transitions as the switching transition. This type of polymers absorb water, and this affects their mechanical and physical properties^{64,65}. The solution molecule has a plasticizing effect on polymeric materials and thus increases the flexibility of the macromolecular chains, leading to a reduction in the transition temperature and resulting in shape recovery. By disrupting the intramolecular H bonding and acting as a plasticizer, water reduce T_g and hence effectively allowed for room temperature actuation⁶⁶. The mechanism behind it is solution firstly intenerates polymeric materials till the T_g of polymer lowered down to the ambient temperature, then hydrogen bonding interaction improves the flexibility of polymeric macro-molecular chains, leading to a SME induced by hydration^{67,68}.

Huang et al. studied water-driven SMPs, their mechanism and influencing factors. It was found that hydrogen bonding was the key behind the water-responsive SMPs, and the water absorbed in the polymer played a main role in the water-driven shape recovery process⁶⁷. Because of the strong interaction between the elastic and transition segments in these polymers, it is difficult to predict their properties (such as the transition/shape recovery temperature and stiffness). It is required individual characterization of their respective properties and behaviors after synthesis^{20,60}.

Water (or moisture)-responsive SMP has been realizes in a couple of polymer systems. A water-responsive programmable SME was observed in SMPUs since their T_g was reduced dramatically after conditioning in water⁵⁸. Another class of materials with potential shape memory behavior in response to relative humidity changes are Poly(methylacrylate) (PMA) copolymers⁶⁹. This polymers display controllable shrinkages activated by increase in relative humidity. Recently Chen et al demonstrated that also chitosan can respond to humidity changes⁷⁰. Focused on the vascular stenting application, they processed spiral coils of chitosan/PEG strands that were then chemically fixed by crosslinking to set the equilibrium shape. The developed stent can

be rapidly expanded from a crimped state to its expanded state, stimulated by hydration in an aqueous environment ⁷¹.

6. Polymeric material with shape memory behavior

A variety of SMPs have been invented and well-documented in the literature, while presently new ones keep on emerging every time. Several polymers, including polyurethane, polynorbornene, styrene-butadiene copolymers, crosslinked polyethylene, and epoxy-based polymers, have been investigated with shape memory behaviors ^{34,72}.

Shape memory polyurethanes (SMPUs) remain one of the main classes of SMPs studied ⁴². Their attractiveness mainly lies in their unique properties, such as a wide range of shape recovery temperatures (from -30 to 70°C), high shape recoverability, good processing ability and excellent biocompatibility ^{73,74}. Many studies reported the use of PU as SMP in various forms such as coil ⁷⁵, foam ⁷⁶, microactuator ⁷⁷ or stents ⁷⁸ for applications in aneurism occlusion, clot removal or intravascular stent. However, recent studies have shown some disadvantages of SMPUs such as their low thermal conductivity, lower mechanical properties, reduction in shape memory performance over the first several thermomechanical cycles and high-thermal-expansion coefficients ^{42,79}.

Other polymer use as shape memory polymer and, like SMPUs, commercially available is the epoxy ¹⁶. Shape memory epoxy possesses excellent shape memory performance, high shape retention ratio, shape recovery ratio and rapid response, and unique thermal, mechanical properties. Its tensile strength, storage modulus and thermal transition temperature can be easily tuned in a large range by varying the formulation ^{42,80}. However, one main disadvantage of the epoxy-based SMPs is related to their high brittleness and low impact strength arising from the highly crosslinked network structure ⁷².

Traditional commercial SMPs, including polyurethane-based and epoxy-based SMPs, were not originally designed for biomedical applications ⁷². Many groups are attempting to develop new SM materials that offer a combination of the follow characteristics: biocompatibility, bioresorbability, biodegradability, and low cytotoxicity, among others ⁴².

Polycaprolactone (PCL) is a kind of biocompatible, biodegradable polymer material and is not toxic to living organisms. PCL has a semicrystalline structure, and its crystalline melting point is 55-60°C. This polymer can be used for shape memory material with lower recoverable temperature. PCL can be used for surgical fixation devices and drug delivery systems^{81,82}.

Since Lendlein and Langer reported a PCL-based biodegradable polymer and demonstrated its potential in medical applications⁸³, biodegradable SMPs become under spot considerable research interest. The biodegradable SMPs is mainly based on polyglycolide (PGA), poly(lactic acid) (PLA) and PCL^{84,85}.

The polymers used as shape memory devices are essentially synthetic polymers. Synthetic polymers are more controllable and predictable than naturally derived polymers, whereas chemical and physical properties of the polymer can be tailored to match specific mechanical and degradation characteristics³. However, they have a lack of biological cues because these materials do not benefit from direct cell-scaffold interactions that could promote the desired cell response. In addition, some degradation products may be toxic or elicit an inflammatory response due to their accumulation and decrease of local pH derived of acidic products⁸⁶.

The growing interests in natural-based polymers relies on their similarities with extracellular matrix (ECM), biocompatibility, biodegradability, low toxicity, low manufacture costs, low disposal costs and renewability^{87,88}. Among the naturally occurring polymers which can be used as such as smart polymers, polysaccharides constitutes a very common and important family of biomolecules⁸⁸.

6.1 Chitosan

Due to their structural and functional similarity to the components found in living tissues, natural-based polymers have been proposed to be used in a series of biomedical applications⁸⁸. Among natural derived polymers, chitin is one of the most abundant organic material, which can be found in shells of marine crustaceans and cell walls of fungi. The most important derivative of it is chitosan^{89,90}. Considerable attention has been given to chitosan (CHT), due to its advantages like low cost, large-scale availability, antimicrobial activity, non-toxicity, biodegradability, and biocompatibility⁹¹⁻⁹³.

This polysaccharide is obtained by a partial deacetylation of chitin (Figure I.7) under alkaline treatment (concentrated sodium hydroxide - NaOH) or by enzymatic hydrolysis in the presence of chitin deacetylase^{92,93}.

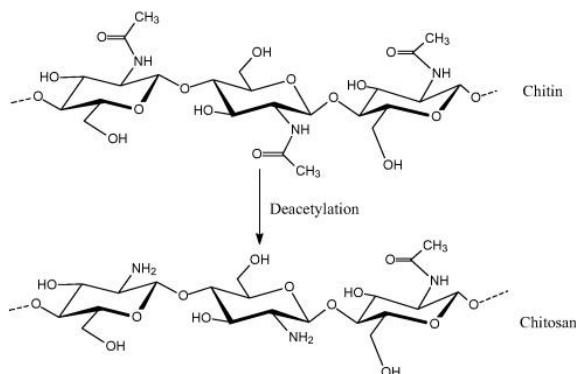


Figure I.7 - Chemical structure of chitin and chitosan⁹⁴.

Structurally, chitosan is a linear polysaccharide consisting of N-glucosamine and N-acetyl glucosamine units available in different grades depending upon the degree of deacetylation, where the two types of repeating units are linked by (1→4)-β-glycosidic bonds⁹⁵. The degree of deacetylation (DD) measures the ratio between glucosamine and N-acetyl glucosamine in polymeric chains, and usually can vary, depending on the source, from 30% to 95%⁹³. Depending on the source and preparation procedure, chitosan molecular weight may range from 300 to over 1000 kDa with a DD from 30% to 95%^{96,97}. DD directly affect the chemical and biological properties of the polymer, such as solubility, crystallinity, swelling behavior and biological properties, namely biodegradation by lysozyme, wound healing properties and enhancement of osteogenesis. The presence of the amine and hydroxyl groups in CHT also permits the incorporation of a variety of chemical groups, enabling its range of properties to be extended, including the possibility of preparing systems that react to external stimuli, such as pH or temperature^{93,97,98}.

Chitosan is degraded by enzymatic hydrolysis being lysozyme the primary agent of *in vivo* degradation⁹⁹. The degradation rate is inversely related to the percentage of crystallinity which is controlled mainly by the degree of deacetylation. Highly deacetylated forms (e.g. 85%) exhibit the lowest degradation rates and may last several months *in vivo*¹⁰⁰.

Chitosan possess many unique properties, such as biocompatibility, biodegradability, antibacterial activity, wound healing properties and easy accessibility¹⁰¹⁻¹⁰⁴. Moreover chitin-based polymers are materials with great versatility to be processed in different structures, such as microspheres, paste, membranes, sponges, fibers and porous scaffolds^{104,105}.

Previous studies showed that Chitosan can undergo a glass transition by the action of hydration^{13,14}. Therefore, we hypothesize that the occurrence of a T_g in chitosan activated by hydration variation could be used in the production of devices with shape memory, that could find interest in the biomedical field.

6.2 SMP Composites

Polymer composites are commonly defined as the combination of a polymer matrix and additives in order to modify the shortcomings of the polymer. The SMPs in general exhibit low strength and stiffness compared to shape memory alloys or ceramics¹⁰⁶. For instance, SMPs have relatively low recovery stress, which is usually 1-3MPa compared to 0.5-1 GPa for SMAs¹⁰⁷. The relatively low recovery stress becomes a limiting factor in many applications especially in cases where SMP devices should overcome a large resisting stress during shape recovery. Thus incorporation of reinforcing elements has been investigated in order to improve the mechanical properties and to diversity the applications of SMPs. Incorporation of filler leads to an improvement in material properties, such as modulus, strength, stiffness and heat resistance^{37,108}. The enhancement of material properties and creation of novel functions has been linked to the interfacial interaction between the polymer matrix and fillers as well the formation of a network of interconnected filler particles²⁸.

The SMP composites can be classified as particle- or fiber-reinforced depending on the type of filler they employ^{37,50}. SMP composites filled with particles, carbon nanotubes, carbon nanofibers, SiC, Ni, Fe₃O₄, and short or continuous fibers may meet various requirements in practical applications^{109,110}. In general, the SMP composites filled with particles or short fiber develop some particular function, such as high electrical conductivity, magnetic-responsive performance, or high stiffness on the micro scale^{37,106}. Among composites, nanocomposites are the most attractive because their size effects result in better performance^{108,109}.

6.2 1. Bioactive Glass Nanoparticles (BG-NPs)

Bioactive materials have the capability to develop a calcium phosphate layer in contact with bone upon implantation and typically exhibit a good integration with this tissue. Examples of bioactive glasses and ceramics are Bioglass®, sintered hydroxyapatite and β -tricalcium phosphate^{111,112}.

Different bioactive ceramics such as calcium phosphates, hydroxyapatite powders, bioactive glass fibres and particles have been used as reinforcing phases in porous biocomposites, mainly for bone-tissue engineering applications^{111,113}. Previous studies show that based on addition of bioactive glass particles to polymer scaffolds, there is improved mechanical properties such as higher compressive strength and modulus^{114,115}. Bioactive glass has shown a rapid biochemical response in physiological fluids ('bioactivity') and, due to improving mechanical properties in polymer based composites, it has proved to be the filler of choice for optimizing such structures to promote tissue growth in bone repair^{113,116}. When exposed to physiological fluids the glass reacts to form tenacious bonds to both hard and soft tissues through cellular activity, demonstrating the bioactivity of this material^{117,118}. Through interfacial and cell mediated reactions, bioactive glass develops a calcium deficient, carbonated phosphate surface layer that allows it to chemically bond to host bone. This bone-bonding behavior is referred to as bioactivity, and has been associated with the formation of a carbonated hydroxyapatite layer on the glass surface when implanted or in contact with biological fluids^{117,119}.

This work presents the development of bioactive composites using BG-NPs as filler in the chitosan scaffolds to fulfill as many requirements as possible, combining advantages of polymers and inorganic components¹¹⁷. We hypothesize that the use of bioactive particles can improve bioactivity, the remineralisation and mechanical properties of new biomaterials due to the increased surface area, which may open new possibilities based on the combination of such materials with polymers in the engineering of bone regeneration^{116,120}.

7. Biomedical Applications of SMPs

The unique properties of SMPs present enormous opportunities for the design of the next generation less invasive, resorbable smart medical implants, tissue scaffolds and medical devices, such as biodegradable sutures, actuators, catheters and smart stents^{121,122}. Since polymers can be made biodegradable they can be used as a short term implants where removal by surgery can be avoided¹⁸.

The development of minimally invasive surgery enabled to place small devices inside the body through a small incision. SMP permit new medical procedure to substitute the complex surgery followed by device implantation^{5,123}. By using the dual-shape properties of SMP, implants could be delivered in the desired target in a compressed, temporary shape, which could go through a small laparoscopic hole. Then, triggered by application of an appropriated stimulus the polymer acquires the functional and permanent shape. After the implant has fulfilled its intended use and tissue regeneration has occurred, the material degrades into substances which can be eliminated by the body, thus allowing full functionality to be restored without the necessity for a second surgery to remove the implant^{18,83}.

Metallic shape memory alloys are already used as cardiovascular stents or guide wires¹²⁴. However, despite of their broad range of applications, SMAs have a limited range of mechanical deformation and remain permanently in the body, causing in some cases, severe complications such as thrombotic occlusions^{4,18}.

The SMP have been proposed for stent applications because of their high strain recovery without the adverse strain hardening effects that is seen in metal stent expansion^{125,126}. Vascular stents are small tubular scaffolds used to maintain the occlusion of an artery. Crimped over a catheter, they are navigated to the lesion site where they are expanded either by balloon expansion or by self-expansion⁴². Moreover the SMP stents have the possibility of embedding drugs within stents to reduce rejection responses⁴², can also be a promise for pediatric stenting in which the stent would grow with the patient, offering an evident competitive advantage over metal stents^{127,128}.

Another application of SMP is smart sutures for wound closure¹²³. The big challenge in endoscopy surgery is manipulated the suture so that the wound lips are pressed together under the right stress. When the knot of a suture is fixed with the wrong force complications such necroses of the tissue or formation of hernias can occur¹⁸. Lendlein and Langer reported a thermoplastic elastomer-based SMP, which can

be used as a smart suture⁸³. A design of smart surgical suture was considered whose temporary shape is obtained by elongating the fiber with controlled stress. This suture is applied loosely in its temporary elongated shape. When the temperature is raised above T_g , the suture shrinks and tightens the knot, applying the optimum force¹²³.

Unlike the large number of neat SMP applications documented, the dominant focus of porous SMPs has been for embolic vascular devices. These devices seek to take advantage of large shape recovery, large surface area to volume ratios, and tortuous flow. Other potential biomedical applications include scaffolds for filling bone defects, hemostatic sponges, soft tissue scaffolds, and drug delivery platforms. These applications take advantage of the volume recovery and surface area advantages of porous SMPs¹⁶.

7.1 Drug delivery Systems

Recently, controlled drug release has been added to the list of functionalities of SMP, leading to multifunctional materials that combine biodegradability, controlled drug release and shape-memory capability¹²⁹⁻¹³¹. This would allow combine the shape-memory effect for enabling minimally invasive implantation bulky devices, biodegradability to avoid a second surgery for implant removal, and controlled drug release for treating infections, reducing inflammatory response or supporting regeneration processes^{7,132,133}. The three major requirements of SMP for drug release applications are maintenance of shape memory functionality after drug incorporation, diffusion release independent of polymer biodegradation, and drug release profiles independent of polymer programming and recovery processes, in order to adapt each individual functionality to the requirements of the application^{9,11}. However, in the preferred case of SMPs with the capability to undergo biodegradation, substantial alterations of polymer properties will occur after exposure to a physiological environment. As a consequence of polymer degradation, implants lose structural integrity¹¹. Depending on the speed and pathway of polymer degradation, drug release and degradation may overlap. Therefore, substantial differences in the involved mechanism of drug release can be expected depending on the type of matrix polymer and its degradation properties^{9,132}.

Expandable stents with drug delivery mechanism have been suggested as a first example for potential applications¹²⁹. Other applications are for contraceptive implants or scaffolds for tissue engineering^{5,132}.

8. Conclusions and Outlook

Although it may be debatable whether SME is an intrinsic polymeric property, its molecular origin clearly suggests that polymer SMEs should not be regarded as properties reserved to a small number of specially designed polymers.

A strong focus will be on SMPs that allow an on-demand control shape recovery so that they can be actuated independently from the body temperature. Moreover, the necessity of implants that are able to perform complex movements will lead to the development of SMPs that can remember multi and complex temporary shapes. The main goal for future SMPs remains the achievement of multifunctional polymers systems that combines SME with biodegradability and controlled drug release.

Tailoring the characteristics of SMPs to meet the specific requirements of targeted applications will continue to be an essential aspect of SMP research. The discovery of novel SMEs will play a significant role as it pushes the material capability into new fields.

9. References

- 1 Chen, Q., Roether, J. & Boccaccini, A. Tissue engineering scaffolds from bioactive glass and composite materials.
- 2 Zhang, Y. & Zhang, M. Three-dimensional macroporous calcium phosphate bioceramics with nested chitosan sponges for load-bearing bone implants. *Journal of biomedical materials research* **61**, 1-8 (2002).
- 3 Dhandayuthapani, B., Yoshida, Y., Maekawa, T. & Kumar, D. S. Polymeric scaffolds in tissue engineering application: a review. *International Journal of Polymer Science* **2011** (2011).
- 4 El Feninat, F., Laroche, G., Fiset, M. & Mantovani, D. Shape memory materials for biomedical applications. *Advanced Engineering Materials* **4**, 91 (2002).
- 5 Lendlein, A., Behl, M., Hiebl, B. & Wischke, C. Shape-memory polymers as a technology platform for biomedical applications. *Expert review of medical devices* **7**, 357-379 (2010).
- 6 Weigel, T., Schinkel, G. & Lendlein, A. Design and preparation of polymeric scaffolds for tissue engineering. *Expert review of medical devices* **3**, 835-851 (2006).
- 7 Neffe, A. T., Hanh, B. D., Steuer, S. & Lendlein, A. Polymer networks combining controlled drug release, biodegradation, and shape memory capability. *Advanced Materials* **21**, 3394-3398 (2009).
- 8 Lendlein, A. *Shape-Memory Polymers*. Vol. 226 (Springer, 2009).

-
- 9 Wischke, C., Neffe, A. T. & Lendlein, A. in *Shape-Memory Polymers* 177-205
(Springer, 2010).
- 10 Behl, M., Razzaq, M. Y. & Lendlein, A. Multifunctional Shape-Memory Polymers.
Advanced Materials **22**, 3388-3410 (2010).
- 11 Serrano, M. C. & Ameer, G. A. Recent Insights Into the Biomedical Applications of
Shape-memory Polymers. *Macromolecular bioscience* **12**, 1156-1171 (2012).
- 12 Liu, F. & Urban, M. W. Recent advances and challenges in designing stimuli-
responsive polymers. *Progress in Polymer Science* **35**, 3-23 (2010).
- 13 Mano, J. F. Viscoelastic properties of chitosan with different hydration degrees as
studied by dynamic mechanical analysis. *Macromolecular bioscience* **8**, 69-76 (2008).
- 14 Caridade, S. G., da Silva, R. M., Reis, R. L. & Mano, J. F. Effect of solvent-dependent
viscoelastic properties of chitosan membranes on the permeation of 2-phenylethanol.
Carbohydrate Polymers **75**, 651-659 (2009).
- 15 Ma, L. *et al.* Collagen/chitosan porous scaffolds with improved biostability for skin
tissue engineering. *Biomaterials* **24**, 4833-4841 (2003).
- 16 Hearon, K. *et al.* Porous Shape-Memory Polymers. *Polymer Reviews* **53**, 41-75 (2013).
- 17 Xie, T. Recent advances in polymer shape memory. *Polymer* **52**, 4985-5000 (2011).
- 18 Ratna, D. & Karger-Kocsis, J. Recent advances in shape memory polymers and
composites: a review. *J Mater Sci* **43**, 254-269 (2008).
- 19 Lendlein, A. & Shastri, V. P. Stimuli-Sensitive Polymers. *Advanced Materials* **22**,
3344-3347, doi:10.1002/adma.201002520 (2010).
- 20 Huang, W. M. *et al.* Shape memory materials. *Materials Today* **13**, 54-61 (2010).
- 21 Chang, L. C. & Read, T. A. Plastic deformation and diffusionless phase changes in
metals — the gold-cadmium beta phase. *Trans AIME* **191**, 47-52 (1951).
- 22 Sun, L. *et al.* Stimulus-responsive shape memory materials: A review. *Materials &*
Design **33**, 577-640 (2012).
- 23 Charlesby, A. Atomic Radiation and Polymers. *Pergamon Press*, 198-257 (1960).
- 24 Otsuka, K. & Wayman, C. M. *Shape memory materials*. (Cambridge University Press,
1999).
- 25 Miyazaki, S., Fu, Y. Q. & Huang, W. M. *Thin film shape memory alloys: fundamentals*
and device applications. (Cambridge University Press, 2009).
- 26 Sun, L. & Huang, W. Thermo/moisture responsive shape-memory polymer for possible
surgery/operation inside living cells in future. *Materials & Design* **31**, 2684-2689
(2010).
- 27 Liu, C., Qin, H. & Mather, P. Review of progress in shape-memory polymers. *Journal*
of Materials Chemistry **17**, 1543-1558 (2007).
- 28 Gunes, I. S. & Jana, S. C. Shape memory polymers and their nanocomposites: a review
of science and technology of new multifunctional materials. *Journal of Nanoscience*
and Nanotechnology **8**, 1616-1637 (2008).
- 29 Yakacki, C. M. *et al.* Strong, Tailored, Biocompatible Shape-Memory Polymer
Networks. *Advanced Functional Materials* **18**, 2428-2435 (2008).
- 30 Lendlein, A., Jiang, H., Jünger, O. & Langer, R. Light-induced shape-memory
polymers. *Nature* **434**, 879-882 (2005).
- 31 Cho, J. W., Kim, J. W., Jung, Y. C. & Goo, N. S. Electroactive shape-memory
polyurethane composites incorporating carbon nanotubes. *Macromolecular Rapid*
Communications **26**, 412-416 (2005).
- 32 Weigel, T., Mohr, R. & Lendlein, A. Investigation of parameters to achieve
temperatures required to initiate the shape-memory effect of magnetic nanocomposites
by inductive heating. *Smart Materials and Structures* **18**, 025011 (2009).
- 33 Ghobadi, E., Heuchel, M., Kratz, K. & Lendlein, A. Influence of the addition of water
to amorphous switching domains on the simulated shape-memory properties of poly (L-
lactide). *Polymer* (2013).
- 34 Lendlein, A. & Kelch, S. Shape-memory polymers. *Angewandte Chemie International*
Edition **41**, 2034-2057 (2002).
- 35 Behl, M. & Lendlein, A. Shape-memory polymers. *Materials Today* **10**, 20-28 (2007).
-

-
- 36 Behl, M. & Lendlein, A. Actively moving polymers. *Soft Matter* **3**, 58-67 (2007).
- 37 Leng, J., Lan, X., Liu, Y. & Du, S. Shape-memory polymers and their composites: stimulus methods and applications. *Progress in Materials Science* **56**, 1077-1135 (2011).
- 38 Rousseau, I. A. Challenges of shape memory polymers: A review of the progress toward overcoming SMP's limitations. *Polymer Engineering & Science* **48**, 2075-2089 (2008).
- 39 Wornyo, E., Gall, K., Yang, F. & King, W. Nanoindentation of shape memory polymer networks. *Polymer* **48**, 3213-3225 (2007).
- 40 Liu, Y., Gall, K., Dunn, M. L., Greenberg, A. R. & Diani, J. Thermomechanics of shape memory polymers: Uniaxial experiments and constitutive modeling. *International Journal of Plasticity* **22**, 279-313 (2006).
- 41 Tobushi, H., Okumura, K., Hayashi, S. & Ito, N. Thermomechanical constitutive model of shape memory polymer. *Mechanics of Materials* **33**, 545-554 (2001).
- 42 Mather, P. T., Luo, X. & Rousseau, I. A. Shape memory polymer research. *Annual Review of Materials Research* **39**, 445-471 (2009).
- 43 Xie, T., Xiao, X. & Cheng, Y.-T. Revealing Triple-Shape Memory Effect by Polymer Bilayers. *Macromolecular Rapid Communications* **30**, 1823-1827 (2009).
- 44 Xie, T. Tunable polymer multi-shape memory effect. *Nature* **464**, 267-270 (2010).
- 45 Meng, H. & Li, G. Reversible switching transitions of stimuli-responsive shape changing polymers. *Journal of Materials Chemistry A* **1**, 7838-7865, doi:10.1039/c3ta10716g (2013).
- 46 Bellin, I., Kelch, S. & Lendlein, A. Dual-shape properties of triple-shape polymer networks with crystallizable network segments and grafted side chains. *Journal of Materials Chemistry* **17**, 2885-2891 (2007).
- 47 Behl, M. & Lendlein, A. Triple-shape polymers. *Journal of Materials Chemistry* **20**, 3335-3345 (2010).
- 48 Bellin, I., Kelch, S., Langer, R. & Lendlein, A. Polymeric triple-shape materials. *Proceedings of the National Academy of Sciences* **103**, 18043-18047 (2006).
- 49 Behl, M., Bellin, I., Kelch, S., Wagermaier, W. & Lendlein, A. One-Step Process for Creating Triple-Shape Capability of AB Polymer Networks. *Advanced Functional Materials* **19**, 102-108 (2009).
- 50 Hu, J., Zhu, Y., Huang, H. & Lu, J. Recent advances in shape-memory polymers: Structure, mechanism, functionality, modeling and applications. *Progress in Polymer Science* **37**, 1720-1763 (2012).
- 51 He, Z., Satarkar, N., Xie, T., Cheng, Y. T. & Hilt, J. Z. Remote controlled multishape polymer nanocomposites with selective radiofrequency actuations. *Advanced Materials* **23**, 3192-3196 (2011).
- 52 Li, J. *et al.* A versatile approach to achieve quintuple-shape memory effect by semi-interpenetrating polymer networks containing broadened glass transition and crystalline segments. *Journal of Materials Chemistry* **21**, 12213-12217 (2011).
- 53 Meng, H. & Hu, J. A brief review of stimulus-active polymers responsive to thermal, light, magnetic, electric, and water/solvent stimuli. *Journal of Intelligent Material Systems and Structures* **21**, 859-885 (2010).
- 54 Zhang, H., Wang, H., Zhong, W. & Du, Q. A novel type of shape memory polymer blend and the shape memory mechanism. *Polymer* **50**, 1596-1601 (2009).
- 55 Chen, S., Hu, J. & Chen, S. Studies of the moisture-sensitive shape memory effect of pyridine-containing polyurethanes. *Polymer International* **61**, 314-320 (2012).
- 56 Niu, G. & Cohn, D. Water Triggered Shape Memory Materials. *Science* **3**, 49-50 (2013).
- 57 Chae Jung, Y., Hwa So, H. & Whan Cho, J. Water-Responsive Shape Memory Polyurethane Block Copolymer Modified with Polyhedral Oligomeric Silsesquioxane. *Journal of Macromolecular Science Part B--Physics* **45**, 453-461 (2006).
-

-
- 58 Huang, W., Yang, B., Zhao, Y. & Ding, Z. Thermo-moisture responsive polyurethane shape-memory polymer and composites: a review. *Journal of Materials Chemistry* **20**, 3367-3381 (2010).
- 59 Du, H. & Zhang, J. Solvent induced shape recovery of shape memory polymer based on chemically cross-linked poly (vinyl alcohol). *Soft Matter* **6**, 3370-3376 (2010).
- 60 Fan, K. *et al.* Water-responsive shape memory hybrid: design concept and demonstration. *Express Polymer Letters* **5**, 409-416 (2011).
- 61 Wang, C. C., Huang, W. M., Ding, Z., Zhao, Y. & Purnawali, H. Cooling-/water-responsive shape memory hybrids. *Composites Science and Technology* **72**, 1178-1182 (2012).
- 62 Yang, B., Huang, W., Li, C. & Li, L. Effects of moisture on the thermomechanical properties of a polyurethane shape memory polymer. *Polymer* **47**, 1348-1356 (2006).
- 63 Yu, Y.-J., Hearon, K., Wilson, T. S. & Maitland, D. J. The effect of moisture absorption on the physical properties of polyurethane shape memory polymer foams. *Smart Materials and Structures* **20**, 085010 (2011).
- 64 Yang, B., Huang, W., Li, C., Lee, C. & Li, L. On the effects of moisture in a polyurethane shape memory polymer. *Smart Materials and Structures* **13**, 191 (2004).
- 65 Pierce, B. F., Bellin, K., Behl, M. & Lendlein, A. Demonstrating the influence of water on shape-memory polymer networks based on poly [(rac-lactide)-co-glycolide] segments in vitro. *International journal of artificial organs* **34**, 172-179 (2011).
- 66 Lv, H., Leng, J., Liu, Y. & Du, S. Shape-Memory Polymer in Response to Solution. *Advanced Engineering Materials* **10**, 592-595 (2008).
- 67 Huang, W., Yang, B., An, L., Li, C. & Chan, Y. Water-driven programmable polyurethane shape memory polymer: demonstration and mechanism. *Applied Physics Letters* **86**, 114105-114105-114103 (2005).
- 68 Du, S. Y., Zhang, D. X., Liu, Y. J., Leng, J. S. & Lv, H. B. Solution-responsive shape-memory polymer driven by forming hydrogen bonding. *Advanced Materials Research* **47**, 258-261 (2008).
- 69 Ishiyama, C. & Higo, Y. Effects of humidity on Young's modulus in poly (methyl methacrylate). *Journal of Polymer Science Part B: Polymer Physics* **40**, 460-465 (2002).
- 70 Jin, J., Song, M. & Hourston, D. Novel chitosan-based films cross-linked by genipin with improved physical properties. *Biomacromolecules* **5**, 162-168 (2004).
- 71 Chen, M.-C. *et al.* Rapidly self-expandable polymeric stents with a shape-memory property. *Biomacromolecules* **8**, 2774-2780 (2007).
- 72 Liu, Y., Han, C., Tan, H. & Du, X. Thermal, mechanical and shape memory properties of shape memory epoxy resin. *Materials Science and Engineering: A* **527**, 2510-2514 (2010).
- 73 Kim, B. K., Lee, S. Y. & Xu, M. Polyurethanes having shape memory effects. *Polymer* **37**, 5781-5793 (1996).
- 74 Zhuohong, Y., Jinlian, H., Yeqiu, L. & Lapyan, Y. The study of crosslinked shape memory polyurethanes. *Materials chemistry and physics* **98**, 368-372 (2006).
- 75 Hampikian, J. M., Heaton, B. C., Tong, F. C., Zhang, Z. & Wong, C. Mechanical and radiographic properties of a shape memory polymer composite for intracranial aneurysm coils. *Materials Science and Engineering: C* **26**, 1373-1379 (2006).
- 76 Metcalfe, A. *et al.* Cold hibernated elastic memory foams for endovascular interventions. *Biomaterials* **24**, 491-497 (2003).
- 77 Maitland, D. J., Metzger, M. F., Schumann, D., Lee, A. & Wilson, T. S. Photothermal properties of shape memory polymer micro-actuators for treating stroke*. *Lasers in surgery and medicine* **30**, 1-11 (2002).
- 78 Baer, G. M. *et al.* Fabrication and in vitro deployment of a laser-activated shape memory polymer vascular stent. *Biomedical engineering online* **6**, 43 (2007).
- 79 Gunes, I. S., Cao, F. & Jana, S. C. Effect of thermal expansion on shape memory behavior of polyurethane and its nanocomposites. *Journal of Polymer Science Part B: Polymer Physics* **46**, 1437-1449 (2008).
-

-
- 80 Merline, J. D., Reghunadhan Nair, C. & Ninan, K. Synthesis, Characterization, Curing and Shape Memory Properties of Epoxy-Polyether System. *Journal of Macromolecular Science, Part A: Pure and Applied Chemistry* **45**, 312-322 (2008).
- 81 Zhu, G., Liang, G., Xu, Q. & Yu, Q. Shape-memory effects of radiation crosslinked poly (ϵ -caprolactone). *Journal of applied polymer science* **90**, 1589-1595 (2003).
- 82 Vroman, I. & Tighzert, L. Biodegradable polymers. *Materials* **2**, 307-344 (2009).
- 83 Lendlein, A. & Langer, R. Biodegradable, elastic shape-memory polymers for potential biomedical applications. *Science* **296**, 1673-1676 (2002).
- 84 Wang, W., Ping, P., Chen, X. & Jing, X. Polylactide-based polyurethane and its shape-memory behavior. *European polymer journal* **42**, 1240-1249 (2006).
- 85 Ravichandran, R., Sundarrajan, S., Venugopal, J. R., Mukherjee, S. & Ramakrishna, S. Advances in polymeric systems for tissue engineering and biomedical applications. *Macromolecular bioscience* **12**, 286-311 (2012).
- 86 Kim, B.-S. *et al.* Design of artificial extracellular matrices for tissue engineering. *Progress in Polymer Science* **36**, 238-268 (2011).
- 87 Dang, J. M. & Leong, K. W. Natural polymers for gene delivery and tissue engineering. *Advanced Drug Delivery Reviews* **58**, 487-499 (2006).
- 88 Reis, R. L. *et al.* *Natural-based polymers for biomedical applications*. (Woodhead Pub., 2008).
- 89 Khor, E. & Lim, L. Y. Implantable applications of chitin and chitosan. *Biomaterials* **24**, 2339-2349 (2003).
- 90 Shi, C. *et al.* Therapeutic potential of chitosan and its derivatives in regenerative medicine. *Journal of Surgical research* **133**, 185-192 (2006).
- 91 VandeVord, P. J. *et al.* Evaluation of the biocompatibility of a chitosan scaffold in mice. *Journal of biomedical materials research* **59**, 585-590 (2002).
- 92 Alves, N. & Mano, J. Chitosan derivatives obtained by chemical modifications for biomedical and environmental applications. *International Journal of Biological Macromolecules* **43**, 401-414 (2008).
- 93 Kim, I.-Y. *et al.* Chitosan and its derivatives for tissue engineering applications. *Biotechnology Advances* **26**, 1-21 (2008).
- 94 Pham, G. D. *et al.* Some biomedical applications of chitosan-based hybrid nanomaterials. *Advances in Natural Sciences: Nanoscience and Nanotechnology* **2**, 045004 (2011).
- 95 Kurita, K. Chemistry and application of chitin and chitosan. *Polymer Degradation and Stability* **59**, 117-120 (1998).
- 96 Madhally, S. V. & Matthew, H. W. Porous chitosan scaffolds for tissue engineering. *Biomaterials* **20**, 1133-1142 (1999).
- 97 Jayakumar, R., Prabakaran, M., Nair, S. & Tamura, H. Novel chitin and chitosan nanofibers in biomedical applications. *Biotechnology Advances* **28**, 142-150 (2010).
- 98 Martins, A. M., Santos, M. I., Azevedo, H. S., Malafaya, P. B. & Reis, R. L. Natural origin scaffolds with *in situ* pore forming capability for bone tissue engineering applications. *Acta Biomaterialia* **4**, 1637-1645 (2008).
- 99 Vårum, K. M., Myhr, M. M., Hjerde, R. J. & Smidsrød, O. In vitro degradation rates of partially *N*-acetylated chitosans in human serum. *Carbohydrate Research* **299**, 99-101 (1997).
- 100 Di Martino, A., Sittering, M. & Risbud, M. V. Chitosan: a versatile biopolymer for orthopaedic tissue-engineering. *Biomaterials* **26**, 5983-5990 (2005).
- 101 Molinaro, G., Leroux, J.-C., Damas, J. & Adam, A. Biocompatibility of thermosensitive chitosan-based hydrogels: an *in vivo* experimental approach to injectable biomaterials. *Biomaterials* **23**, 2717-2722 (2002).
- 102 No, H. K., Young Park, N., Ho Lee, S. & Meyers, S. P. Antibacterial activity of chitosans and chitosan oligomers with different molecular weights. *International journal of food microbiology* **74**, 65-72 (2002).
- 103 Sall, K., Kreter, J. & Keates, R. The effect of chitosan on corneal wound healing. *Annals of ophthalmology* **19**, 31 (1987).
-

-
- 104 Costa-Pinto, A. R., Reis, R. L. & Neves, N. M. Scaffolds based bone tissue engineering: the role of chitosan. *Tissue Engineering Part B: Reviews* **17**, 331-347 (2011).
- 105 Mano, J. *et al.* Natural origin biodegradable systems in tissue engineering and regenerative medicine: present status and some moving trends. *Journal of the Royal Society Interface* **4**, 999-1030 (2007).
- 106 Liu, Y., Lv, H., Lan, X., Leng, J. & Du, S. Review of electro-active shape-memory polymer composite. *Composites Science and Technology* **69**, 2064-2068 (2009).
- 107 Meng, Q. & Hu, J. A review of shape memory polymer composites and blends. *Composites Part A: Applied Science and Manufacturing* **40**, 1661-1672 (2009).
- 108 Gall, K. *et al.* Shape memory polymer nanocomposites. *Acta Materialia* **50**, 5115-5126 (2002).
- 109 Balazs, A. C., Emrick, T. & Russell, T. P. Nanoparticle polymer composites: where two small worlds meet. *Science* **314**, 1107-1110 (2006).
- 110 Manias, E. Nanocomposites: Stiffer by design. *Nature materials* **6**, 9-11 (2007).
- 111 Kokubo, T. & Kaisha, N. M. M. K. *Bioceramics and their clinical applications*. (Woodhead Pub. and Maney Pub., 2008).
- 112 Luz, G. M. & Mano, J. F. Biomimetic design of materials and biomaterials inspired by the structure of nacre. *Philosophical Transactions of the Royal Society A: Mathematical, Physical and Engineering Sciences* **367**, 1587-1605 (2009).
- 113 Luz, G. M. & Mano, J. F. Chitosan/bioactive glass nanoparticles composites for biomedical applications. *Biomedical Materials* **7**, 054104 (2012).
- 114 Ramakrishna, S., Mayer, J., Wintermantel, E. & Leong, K. W. Biomedical applications of polymer-composite materials: a review. *Composites Science and Technology* **61**, 1189-1224 (2001).
- 115 Kokubo, T., Kim, H.-M. & Kawashita, M. Novel bioactive materials with different mechanical properties. *Biomaterials* **24**, 2161-2175, doi:10.1016/s0142-9612(03)00044-9 (2003).
- 116 Liang, S.-L., Cook, W. D., Thouas, G. A. & Chen, Q.-Z. The mechanical characteristics and *in vitro* biocompatibility of poly (glycerol sebacate)-Bioglass[®] elastomeric composites. *Biomaterials* **31**, 8516-8529 (2010).
- 117 Rezwani, K., Chen, Q., Blaker, J. & Boccaccini, A. R. Biodegradable and bioactive porous polymer/inorganic composite scaffolds for bone tissue engineering. *Biomaterials* **27**, 3413-3431 (2006).
- 118 Luz, G. M. & Mano, J. F. Preparation and characterization of bioactive glass nanoparticles prepared by sol-gel for biomedical applications. *Nanotechnology* **22**, 494014 (2011).
- 119 Zhitomirsky, D., Roether, J., Boccaccini, A. & Zhitomirsky, I. Electrophoretic deposition of bioactive glass/polymer composite coatings with and without HA nanoparticle inclusions for biomedical applications. *Journal of Materials Processing Technology* **209**, 1853-1860 (2009).
- 120 Misra, S. K. *et al.* Comparison of nanoscale and microscale bioactive glass on the properties of P (3HB)/Bioglass[®] composites. *Biomaterials* **29**, 1750-1761 (2008).
- 121 Langer, R. & Tirrell, D. A. Designing materials for biology and medicine. *Nature* **428**, 487-492 (2004).
- 122 Contreras-García, A. & Bucio, E. Biomedical Devices Based on Smart Polymers. *Responsive Materials and Methods: State-of-the-Art Stimuli-Responsive Materials and Their Applications*, 105-122 (2013).
- 123 Sokolowski, W., Metcalfe, A., Hayashi, S., Yahia, L. H. & Raymond, J. Medical applications of shape memory polymers. *Biomedical Materials* **2**, S23 (2007).
- 124 Lendlein, A. & Kelch, S. Shape-memory polymers as stimuli-sensitive implant materials. *Clinical hemorheology and microcirculation* **32**, 105-116 (2005).
- 125 Tamai, H. *et al.* Initial and 6-month results of biodegradable poly-l-lactic acid coronary stents in humans. *Circulation* **102**, 399-404 (2000).
- 126 Vogt, F. *et al.* Long-term assessment of a novel biodegradable paclitaxel-eluting coronary polylactide stent. *European heart journal* **25**, 1330-1340 (2004).
-

-
- 127 Yakacki, C. M. *et al.* Unconstrained recovery characterization of shape-memory polymer networks for cardiovascular applications. *Biomaterials* **28**, 2255-2263 (2007).
- 128 Yakacki, C. M., Willis, S., Luders, C. & Gall, K. Deformation Limits in Shape-Memory Polymers. *Advanced Engineering Materials* **10**, 112-119 (2008).
- 129 Wache, H., Tartakowska, D., Hentrich, A. & Wagner, M. Development of a polymer stent with shape memory effect as a drug delivery system. *Journal of Materials Science: Materials in Medicine* **14**, 109-112 (2003).
- 130 Neffe, A. T., Hanh, B. D., Steuer, S., Wischke, C. & Lendlein, A. in *Mater. Res. Soc. Symp. Proc.* 105-111 (Cambridge Univ Press).
- 131 Wischke, C. & Lendlein, A. Shape-memory polymers as drug carriers—a multifunctional system. *Pharmaceutical research* **27**, 527-529 (2010).
- 132 Wischke, C., Neffe, A. T., Steuer, S. & Lendlein, A. Evaluation of a degradable shape-memory polymer network as matrix for controlled drug release. *Journal of Controlled Release* **138**, 243-250 (2009).
- 133 Nagahama, K., Ueda, Y., Ouchi, T. & Ohya, Y. Biodegradable shape-memory polymers exhibiting sharp thermal transitions and controlled drug release. *Biomacromolecules* **10**, 1789-1794 (2009).

Chapter II. - Materials and Methods

1. Materials

Chitosan (CHT) of medium molecular weight ($M_w = 190.000-310.000$, 75-85% Degree of deacetylation, viscosity 200-800 cps) and Congo Red were purchased from Sigma Aldrich. Genipin was a product of Wako Chemicals. Tetraethyl orthosilicate (TEO) (99.90% pure), ammonium phosphate dibasic, calcium nitrate tetrahydrate (99%), citric acid monohydrate (99–100%), ammonium hydroxide (maximum 33% NH_3) and poly(ethylene glycol) used for BG-NPs production and all chemicals for SBF preparation were purchased from Sigma–Aldrich. All other chemicals were reagent grade and were used as received.

2. Methods**2.1 Chitosan Purification**

Prior to any use, commercial chitosan of medium molecular weight was purified by reprecipitation method. A solution of 1% (w/v) chitosan and 2% (v/v) acetic acid was prepared and then filtered: first with a nylon filter followed by two filtrations with paper filter (20-25 μm). This solution was precipitated by adding 2M aqueous sodium hydroxide (NaOH) until pH reached 8. The chitosan flakes was washed with distilled water until neutralize, and dehydrated with water/ethanol solutions with percentages of 80/20, 50/50 and 10/90. Finally, the chitosan flakes were frozen, freeze-dried and triturated till a fine powder was obtained.

2.2 Chitosan scaffolds preparation

A solution of 2% (v/v) acetic acid and 3% (w/v) purified Chitosan, was prepared with stirring until homogeneity was reached. The solution is cast into silicone tubes with diameter of 5 mm, working as a mold, and frozen by immersion into liquid

nitrogen. The frozen solution is subsequently freeze-dried to remove the dispersed ice crystals. After freeze-dried, the polymeric structure were neutralized in 1M sodium hydroxide solution (NaOH) for 1hour and freeze-dried again. Then, the tubes were cut in 7 mm pieces, resulting in solidified porous polymeric scaffold with a dimension of 7 mm x Ø5 mm.

2.3 Genipin-crosslinked Chitosan Scaffolds

Crosslinking is an effective and convenient technique to improve the mechanical properties of chitosan. However the most common synthetic chemical used as a crosslinking reagent are chemically synthesized and are not free from the problems caused by physiological toxicity. On the other hand, genipin is an effective naturally occurring-crosslinking agent and can react spontaneously with amino acids or proteins to form dark blue pigments ¹.

Chitosan powder was dissolved at a concentration of 3% (w/v) in aqueous acetic acid 2% (v/v). 3 wt % of genipin (chitosan/genipin = 100/3 by weight) was dissolved in 2 ml of ethanol and then was added to the chitosan solution under constant stirring for 5min at room temperature. The solution was cast into the same tubes used for un-crosslinked chitosan scaffolds and put at 37°C for 4hours. After the reaction occurs, the solution turns dark blue and become increasingly viscous. The tubes are then frozen and is followed the same steps proceeded with the un-crosslinked scaffolds.

2.4 Bioglass nanoparticles (BG-NPs) preparation

To prepare the BG-NPs a protocol based on previous work was followed ². The procedure for preparation of the ternary form of BG-NPs, composed by SiO₂:CaO:P₂O₅ (mol%) = 55:40:5, consisted in sequential reagent dissolutions that resulted in hydrolysis and polycondensation reactions. Tetraethyl orthosilicate (TEOS, 99.90% pure) was used as the Si precursor, ammonium hydrogen phosphate as the P precursor, calcium nitrate tetrahydrate (99%) as the Ca precursor, citric acid monohydrate (99-100%) to promote hydrolysis, absolute ethanol, ammonium hydroxide (maximum of 33% NH₃) as the jellyfying agent and polyethylene glycol 20000 (PEG) as the surfactant. The mixture of precursor's solutions (7.639 g of calcium nitrate in 120 ml of distilled water, 9.167 g of TEOS in 60 ml of ethanol/ 30 ml of citric acid 10% (w/v)) was added drop-by-drop to an aqueous solution containing the phosphorous precursor

(1.078 g of ammonium hydrogen phosphate in 1500 ml of distilled water). The pH was adjusted at 11.5 with ammonium hydroxide addition. The precipitate obtained was stirred for 48h, and then a resting period of 24h followed. The precipitate was washed three times with distilled water. A 200 ml amount of an aqueous solution of Polyethylene glycol 20000 (PEG) was added to the precipitate, and then followed by freeze drying. Finally, the gel powder was calcinated at 700 °C for 5h to get the white bioactive glass nanoparticles.

2.5 Chitosan/BG-NPs Scaffolds preparation

A solution of 2% (v/v) acetic acid in water, 0.7% (w/v) CHT purified and 0.3% (w/v%) BG-NPs, was prepared with stirring until homogeneity was reached. After that the solution was cast into the same tubes used for chitosan scaffolds and followed the same protocol.

2.6 Scanning Electron Microscopy (SEM)

All the developed chitosan based scaffolds were evaluated by scanning electron microscopy (SEM). Moreover, the morphology of CHT/BG-NPs scaffolds after bioactivity test was also evaluated by SEM. This methodology is extremely important to study the morphology of polymeric materials and structures. This technique allows analyzing the morphology of the specimen at large magnifications and also the details of the structure up to the sub-micron level. The morphology of sample surfaces was study by scan electron microscopy (NanoSEM FEI Nova 200 (FEG/SEM)). All samples were coated by gold sputtering for 2 min at a current of 15 mA.

2.7 Porosity measurements

The porosity of the scaffolds is obtained from the density of chitosan and the density of actual porous scaffolds sample produced. The density of chitosan (ρ) is 1.342 g/cm³. So the calculation formula of porosity is defined as:

$$porosity (\%) = \frac{V_m - (W_m/\rho)}{V_m} \times 100 \quad (1)$$

where, V_m is the total volume of chitosan scaffolds (cm³), and W_m is the mass of the scaffold (g).

2.8 Energy Dispersive Spectroscopy (EDS)

Energy dispersive spectroscopy (EDS) methodology was used to detect the presence of calcium (Ca) and phosphorous (P) elements by analyzing the surface of the scaffolds. These two chemical elements are constituents of the mineral phase (hydroxyapatite) of bone ECM. Their presence positively indicates the formation of an apatite layer in the surface of the scaffold. We analyzed the surface of chitosan/BG-NPs scaffolds upon immerse in simulated body fluid (SBF) during 0, 3 and 7 days. The samples were processed as described previously for SEM and the surface of the samples were analyzed by EDS with a Leica Cambridge S360 scanning electron microscope.

2.9 Fourier Transform Infrared Spectroscopy (FTIR)

In Fourier transform infrared spectroscopy (FTIR), infrared radiation will be applied to a sample. The information resulting from radiation absorption or transmitted will give details about the molecular structures present in the sample since only specific molecular vibrations can be excited³.

FTIR analyses were applied to study the composition of the scaffolds. The infrared spectrum was measured using a FTIR Spectrometer (model IRPrestige-21, Shimadzu; Germany) in the wavelength range of 4400–400 cm^{-1} . The samples were combined with potassium bromide (KBr) to produce discs.

2.10 Swelling Properties

The swelling of scaffolds for different contents of water was determined by immersing previously weighted CHT scaffolds in different compositions of water/ethanol mixtures varying from pure water to pure ethanol at room temperature, for 4h. It was confirmed that after a 4h period the scaffolds had reached their swelling equilibrium. After around 4h, swelled samples were blotted with filter paper to remove surface adsorbed solvent and weighted immediately. The swelling ratio was calculated using the following equation:

$$S(\text{wt. \%}) = \frac{(w-w_0)}{w_0} \times 100 \quad (2)$$

where, w and w_0 are the weights of the scaffolds at the swelling state and at the dry state, respectively. Each swelling experiment condition was performed in triplicate.

2.11 Hydromechanical Cyclic Compression Tests

The hydromechanical behavior of the SMPs can be studied by compressive test⁴. The compressive tests of the developed scaffolds were performed using a Universal tensile testing machine (Instron 4505 Universal Machine, USA). The tests were performed under compressive loading, by performing uniaxial compression, using a crosshead speed of $2 \text{ mm}\cdot\text{min}^{-1}$, at a room temperature. The results presented are the average of at least three specimens.

Each specimen measured 7 mm in the direction of testing and 5 mm square in cross-section. The samples were immersed in water for 1h before the test. The tests were performed for different maximum strains ($\epsilon_m = 10, 20, 30$ and 60%).

After the compression test and maintaining the strain, the stress is then held constant while the sample is dehydrated by immersing the sample in ethanol for 20 min, whereby the temporary shape is fixed. Then, the stress is completely removed and the sample is now in its temporary shape. Finally, the samples were immersed in different mixtures of water/ethanol, varying from pure water to pure ethanol, to assess the shape memory recovery. Figure II.1 shows the scheme of the procedure described the scaffolds as a shape memory polymer.

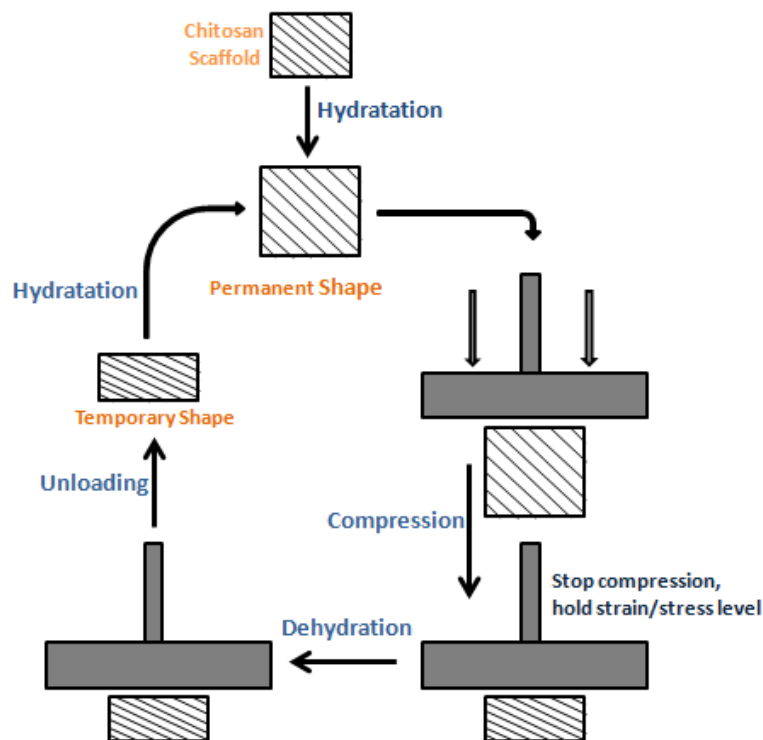


Figure II.1 - Schematic of the programming and recovery process of the SME.

In a hydromechanical compressive cycle, the shape memory capability of the SMP is typically characterized by the shape fixity ratio (R_f) and the shape recovery ratio (R_r). R_f characterizes the ability of a system to fix its temporary shape and R_r is the recoverability of the permanent shape. Shape fixity can be quantified from the following equation,

$$R_f(N) = \frac{\epsilon_u(N)}{\epsilon_m} \quad (3)$$

where, ϵ_u represents the temporary shape strain and ϵ_m represents the applied maximum strain. They are given by,

$$\epsilon_u = \frac{l_0 - l_2}{l_0} \quad \text{and} \quad \epsilon_m = \frac{l_0 - l_1}{l_0} \quad (4)$$

where, l_0 is the initial length, l_1 is the length after compression but before unloading, and l_2 is the length of the temporary shape. Therefore, for one cycle ($N=1$), the shape fixity can be written as,

$$R_f(\%) = \frac{l_0 - l_2}{l_0 - l_1} \times 100 \quad (5)$$

The strain recovery rate quantifies the ability to restore the mechanical deformation of the permanent shape ϵ_p after application of a certain deformation ϵ_m .

For N cycles, the shape recovery is defined as,

$$R_r(N) = \frac{\epsilon_m - \epsilon_p(N)}{\epsilon_m - \epsilon_p(N-1)} \quad (6)$$

where, ϵ_p is the strain associated with the permanent shape given by,

$$\epsilon_p = \frac{l_0 - l_3}{l_0} \quad (7)$$

where, l_3 is the measured length after recovery. For one cycle, the ϵ_p in the denominator goes to zero and the shape recovery is

$$R_r(\%) = \frac{l_3 - l_1}{l_0 - l_1} \times 100 \quad (8)$$

The measures were performed with a digital micrometer.

The change of the Young's modulus (E) with the content of water was also observed. The scaffolds were immersed in different mixtures of water/ethanol for one hour followed by compression load. Thus the stress-strain curve was obtained by performing compressive load until 30% strain. E was determined in the most linear region of the stress–strain graph using the tangent method.

2.11.1 Recovery vs time

The scaffolds recovery along time was evaluated to see how the hydrated scaffolds recovery after being submitted to compression loading. The scaffolds were initially immersed in water and measured, and then a compression test was performed for different maximum strains ($\epsilon_m = 10, 20$ and 30%). After the test the sample was immersed again in water and the samples height was measured in different time points. The strain recovery for a determined time point (t) is:

$$R_t(\%) = \frac{l_t - l_1}{l_0 - l_1} \times 100 \quad (9)$$

2.12 Dynamic Mechanical Analysis (DMA)

Dynamic Mechanical Analysis (DMA) can be employed to measure numerous temperature and frequency-dependent viscoelastic properties of polymers, including glassy and rubbery modulus, which are very important properties for SMPs. DMA is a technique where a small deformation is applied to a sample in a cyclic manner. This allows the materials response to stress, temperature, frequency and other values to be studied. From these measurements it is possible to calculate the storage modulus (E') and the loss factor ($\tan \delta$) versus time or temperature for one or more frequencies⁵.

For this study, compression tests were carried out by dynamic mechanical analysis (DMA) using a Tritec 2000B equipment (Triton Technology, UK). The measurements were carried out at room temperature (20°C).

Un-crosslinked and crosslinked chitosan scaffolds were tested at constant frequency (0.5 Hz and 1 Hz) following the changes in the storage modulus (E') and loss factor ($\tan \delta$) as function of the water content. The dried samples of known geometry were placed in a Teflon[®] reservoir and immersed in a certain volume of ethanol ($V_{\text{eth}} = 270 \text{ ml}$) and kept under the testing constant strain amplitude ($30 \mu\text{m}$) during 30 min.

After this step, E' reached an equilibrium value. Finally, the water was pumped into the reservoir at a constant flow rate ($Q = 14$ ml/min), providing a time (t) dependent change in the content of water described by the following equation:

$$\text{water (vol. \%)} = \frac{Qt}{Qt + V_{eth}} \quad (10)$$

Note that in these measurements E' should be taken as an apparent value as during introduction of water the geometry of the sample continuously changes due to swelling and the calculation of this parameter used the initial geometry of the sample.

2.13 X-ray diffraction measurements

X-ray diffraction (XRD) is employed to characterize the phase composition and percent crystallinity in materials. Crystallinity and phase content of chitosan scaffolds immersed in mixtures of water/ethanol with different compositions (100, 75, 50, 25 and 0% of water content), were investigated with XRD analysis, using an X-ray diffractometer (Bruker D8 Discover). XRD patterns were examined in the region of 5–65° with a step size 0.02° for 2θ and a counting time of 2s step⁻¹.

2.14 *In vitro* drug delivery studies

To study the capability of the chitosan-based scaffolds to be used as a drug delivery device *in vitro* drug studies were performed. In this work, Congo Red was used as a model molecule to investigate the loading and release ability of the scaffold. The choice of the dye was influenced by the humidity-trigger shape memory effect. Congo red is water soluble and presents a low solubility in ethanol⁶. The drug loading was incorporated by swelling. The swelling of the network in drug solutions at room temperature leads to dissolution of the drug in the polymer matrix⁷.

To perform drug delivery studies it is important to know the incorporation efficiency (IE) of the scaffolds. The incorporation efficiency can be measured by the ratio of the drug available for release and the initial loaded drug,

$$IE = \frac{\text{drug available for release}}{\text{loaded drug}} \times 100 \quad (11)$$

The scaffold was immersed in a solution of CR in PBS of 1mg/ml for 1h. The loaded drug was estimated using the variation of the mass of the scaffold during the swelling. Then, the loaded scaffolds were compressed ($\epsilon_m=30\%$) and dehydrated follow by immersion in 5ml of PBS under sonication at 37°C for 5 days to induce a forced release, obtaining the maximum drug release. Such experiment permitted to estimate the total drug available for release in the scaffolds. The amount of CR was quantified spectrophotometrically, measuring the UV absorbance at 498nm (Synergie HT, Bio-Tek, USA) and using a calibration curve generated by absorption measurements of CR solutions with pre-defined concentrations (Figure II.2).

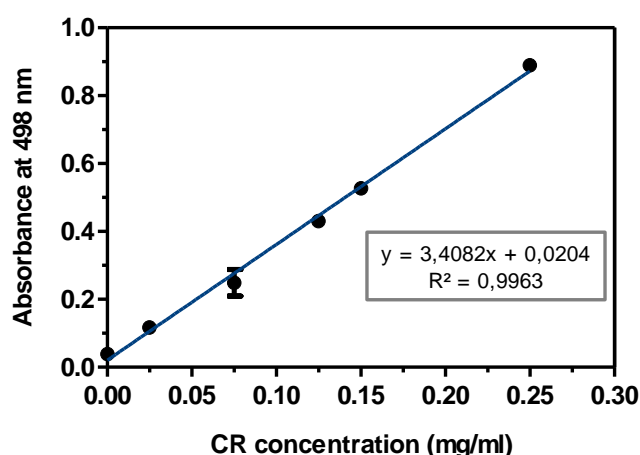


Figure II.2 - Calibration Curve of Absorbance of Congo Red.

To procedure the loading, the samples were immersed in a solution of CR in PBS of 5mg/ml for a period of 1h. After the hydration/loading the samples were compressed ($\epsilon_m=30\%$) and dehydrated for 20 min in ethanol, followed by the evaporation of the solvent. After the deformation and fixation of the temporary shape, both CHT0 and CHT1 were immersed in 5ml of PBS, pH 7.4. The vials containing the scaffolds were kept under agitation (at approximately 60 rpm) in a water bath at 37°C. At pre-established periods of time, aliquots of 1ml of the supernatant were taken out and replaced with equal volume of fresh PBS to maintain the volume constant during the release study. The amount of CR was quantified spectrophotometrically by the same procedure use to measure the IE.

2.15 *In vitro* bioactivity study

The *in vivo* formation of an apatite layer on the surface of a bioactive ceramic can be reproduced in a protein-free and a cellular simulated body fluid (SBF), which is prepared to have an ion concentration nearly equal to that of human blood plasma. Table II.1 compares the ion concentration of SBF and human blood plasma ⁸.

The bioactivity of a biomaterial can be evaluated by examining the formation of apatite on its surface in SBF ⁹. Bioactivity is considered a critical factor in facilitating the chemical fixation of a biomaterial to bone tissue, and ultimately the *in vivo* success of bone grafting material ¹⁰. *In vitro* bioactivity tests were carried out by soaking a CHT/BG-NPs scaffold in 20 ml of SBF for 3 and 7 days at 37°C. Upon removing from SBF the samples were rinsed with distilled water and left to dry.

SBF solution was prepared by dissolving NaCl, NaHCO₃, KCl, K₂HPO₄·3H₂O, MgCl₂·6H₂O and Na₂SO₄ in distilled water and buffered with Tris buffer and HCl to reach a pH value of 7.4, following the protocol described by Kokubo and Takadama ⁸.

Table II.1 - Comparison between ion concentration in SBF and in human blood plasma

Ion	Ion Concentrations (mM)	
	Blood plasma	SBF
Na ⁺	142.0	142.0
K ⁺	5.0	5.0
Mg ²⁺	1.5	1.5
Ca ²⁺	2.5	2.5
Cl ⁻	103.0	147.8
HCO ₃ ⁻	27.0	4.2
HPO ₄ ²⁻	1.0	1.0
SO ₄ ²⁻	0.5	0.5
pH	7.2-7.4	7.4

2.16 Micro-Computed Tomography (μ-CT)

The shape recovery of the BG-NPs scaffolds inside the bone defect produced in the pig femur bone was evaluated by micro-computerized tomography using a Scanco 20 equipment (Skyscan 1702, Belgium) with penetrative X-rays of 40 keV. The X-ray scans were acquired in high-resolution mode. CT Analyser® was used to visualize the

2D X-ray sections images of the scaffolds. Defects were produced in fresh bones by drilling cylindrical holes with a diameter of 4mm.

3. References

- 1 Jin, J., Song, M. & Hourston, D. Novel chitosan-based films cross-linked by genipin with improved physical properties. *Biomacromolecules* **5**, 162-168 (2004).
- 2 Luz, G. M. & Mano, J. F. Preparation and characterization of bioactive glass nanoparticles prepared by sol-gel for biomedical applications. *Nanotechnology* **22**, 494014 (2011).
- 3 Griffiths, P. & De Haseth, J. A. *Fourier transform infrared spectrometry*. Vol. 171 (John Wiley & Sons, 2007).
- 4 Liu, Y., Gall, K., Dunn, M. L., Greenberg, A. R. & Diani, J. Thermomechanics of shape memory polymers: Uniaxial experiments and constitutive modeling. *International Journal of Plasticity* **22**, 279-313 (2006).
- 5 Menard, K. P. *Dynamic mechanical analysis: a practical introduction*. (CRC press, 2008).
- 6 Teather, R. M. & Wood, P. J. Use of Congo red-polysaccharide interactions in enumeration and characterization of cellulolytic bacteria from the bovine rumen. *Applied and environmental microbiology* **43**, 777-780 (1982).
- 7 Neffe, A. T., Hanh, B. D., Steuer, S. & Lendlein, A. Polymer networks combining controlled drug release, biodegradation, and shape memory capability. *Advanced Materials* **21**, 3394-3398 (2009).
- 8 Kokubo, T. & Takadama, H. How useful is SBF in predicting in vivo bone bioactivity? *Biomaterials* **27**, 2907-2915, doi:10.1016/j.biomaterials.2006.01.017 (2006).
- 9 Kokubo, T., Kim, H.-M. & Kawashita, M. Novel bioactive materials with different mechanical properties. *Biomaterials* **24**, 2161-2175 (2003).
- 10 Lu, H. H., El-Amin, S. F., Scott, K. D. & Laurencin, C. T. Three-dimensional, bioactive, biodegradable, polymer-bioactive glass composite scaffolds with improved mechanical properties support collagen synthesis and mineralization of human osteoblast-like cells in vitro. *J Biomed Mater Res A* **64**, 465-474 (2003).

Chapter III. - Chitosan Scaffolds with Shape Memory induced by Hydration

Chitosan Scaffolds with Shape Memory induced by Hydration

Cristina O. Correia ^{1,2}, and João F. Mano, Ph.D ^{1,2}.

1 3B's Research Group – Biomaterials, Biodegradables and Biomimetics; Department of Polymer Engineering, University of Minho; Headquarters of the European Institute of Excellence on Tissue Engineering and Regenerative Medicine; AvePark, Zona Industrial da Gandra S. Cláudio do Barco, 4806-909 Caldas das Taipas, Guimarães, Portugal

2 ICVS/3B's, PT Government Associate Laboratory, Braga/Guimarães, Portugal

Abstract

We demonstrate that chitosan-based porous scaffolds can present a shape memory effect triggered by hydration. The shape memory effect of non-crosslinked (CHT0) and genipin-crosslinked (CHT1) scaffolds was followed by hydromechanical compressive test and dynamic mechanical analysis (DMA), while the sample was immersed in varying compositions of water/ethanol mixtures. By dehydration with higher contents of ethanol, the vitreous-like nature of the amorphous component of chitosan allows the fixation of the temporary shape of the scaffold. The presence of water disrupts inter-molecular hydrogen bonds permitting segmental mobility of the chitosan chains upon the occurrence of the glass transition and thus the recovery of the permanent shape of a pre-deformed scaffold. SEM, swelling tests and XRD analysis were also performed. Results showed that chitosan possess shape memory properties, characterized by a fixity ratio above 97.2% for CHT0 and above 99.2% for CHT1 and a recovery ratio above 70.5% for CHT0 and 98.5% for CHT1. *In vitro* drug delivery studies were also performed to demonstrate that such devices can be also loaded with molecules. We show that the developed chitosan scaffolds are candidates for applications in minimally invasive surgery for tissue regeneration or for drug delivery.

Keywords: chitosan, scaffold, shape memory, hydration.

1. Introduction

The rapid progress in the development of surgical techniques, especially in minimally invasive surgery, leads to more complex requirements for modern implants. Aside the important properties like biocompatible and, ideally in many cases, degradability, the shape memory effect (SME) as a novel functionality of polymers might enable the development of novel types of medical devices¹⁻³. Shape memory polymers (SMPs) offer novel materials-based devices to solving scientific challenges due to their demonstrated ability to actively undergo geometric transformations upon exposure to environmental stimuli^{4,5}.

A shape-memory polymer can be deformed by application of an external stress and fixed in a second shape, the temporary shape. This temporary shape is retained until the shaped body is exposed to an appropriate stimulus, which induces the recovery of the original shape⁴. A impulsive force such as physical or chemical crosslinking points is require for the SME to recover the initial shape after deformation and fixing⁶. SMP can utilize glass transition (T_g)⁷ and/or melting points (T_m)⁸ as the deformation/fixing temperatures. SMP contain a network architecture consisting of netpoints that are connected with stimuli-sensitive macromolecular chains. The netpoints determine the permanent shape and the segment chains are using as a kind of molecular switch. Above the transition temperature the switchable segments gives flexibility for the deformation; under this temperature the segments give stiffness for shape fixation⁹. Besides the temperature, the shape memory technologies can also use other stimulus, such as hydration¹⁰, light¹¹, electromagnetic¹² or electrical¹³. In the present, the most attractive SMPs are still triggered by temperature¹⁴. Thermal-responsive SMP is normally driven by external heat being an issue for applications with restricted temperature ranges like in the biomedical field¹⁵. Non-thermally induced shape memory polymers eliminate the temperature constrains and enable the manipulation of the shape recovered under ambient temperature¹⁶.

Recent studies have shown that the environmental conditions such as the humidity can substantially influence conformational mobility of macromolecular chains, and thus the shape memory properties of polymers¹⁷⁻²⁰. These findings motivated the development of the concept of a moisture triggered SME.

Water or solvent-driven shape recovery effects have been observed in SMPs having glass transitions as switching transition. This type of polymers absorb water, and this affects their mechanical and physical properties^{21,22}. By disrupting intramolecular hydrogen bonds and acting as a plasticizer, water reduce the glass transition and hence effectively allowed for room temperature actuation²³.

Shape memory polymers are ideal candidates for biomedical applications in which a temporary shape has to be preserved until the device is placed in the cavity to be filled, allowing minimally invasive surgical procedures^{24,25}. However most of the polymers studied with shape memory properties are non biodegradable. It is often important that medical polymers are biodegradable in order to avoid a secondary surgery to be removed from the body. Polymers combining degradability with shape memory capability are multifunctional materials. Recently, controlled drug release has been added to the list of functionalities of SMP^{1,26}.

Chitosan (CHT) is a partially N-deacetylated derivative of chitin²⁷. Considerable attention has been given to this polymer due to its advantages like low cost, large-scale availability, antimicrobial activity, non-toxicity, biodegradability, and biocompatibility²⁷⁻²⁹. Chitosan can be processed into scaffolds using different processing techniques to be used in tissue engineering^{30,31}.

The goal of this work is to develop CHT-based scaffolds with shape memory properties. It was found before that CHT can undergo a glass transition by the action of hydration^{32,33}. By combining such effect with the maintenance of the structural integrity of the system (provided by crosslinking or due to the intrinsic semi-crystalline structure) we hypothesize that we could develop new devices in which the recovery of the geometry can be induced by hydration. To control this parameter the tests were conducted in water/ethanol mixtures with distinct compositions. Moreover, the capability of drug delivery was studied in order to achieve multifunctional devices that combine SME, biodegradability and drug delivery ability.

2. Materials and Methods

2.1 Materials

Chitosan (CHT) of medium molecular weight ($M_w= 190.000-310.000$, 75-85% Degree of deacetylation, viscosity 200-800 cps) was purchased from Sigma Aldrich. Before being used CHT was purified by reprecipitation method. CHT powder was dissolved at a concentration of 1% (w/v) in 2% (v/v) aqueous acetic acid and precipitated with a NaOH solution (final pH ~8). The CHT flakes were washed with distilled water until neutralization and dehydrated with ethanol. Finally, the CHT flakes were frozen and lyophilized. Genipin was a product of Wako Chemicals. Congo Red was purchased from Sigma Aldrich. All other chemicals were reagent grade and were used as received.

2.2 Methods

2.2.1 Chitosan Scaffolds Preparation

CHT was dissolved in an aqueous acetic acid solution 2% (v/v) to a concentration of 3% (w/v) with stirring until homogeneity was reached. For the crosslinked system (CHT1), 3 wt % of genipin (chitosan/genipin=100/3 w/w) was added to the CHT solution under stirring. Non-crosslinked CHT scaffolds (CHT0) were prepared directly from the original CHT solutions, with no addition of genipin. In order to obtain scaffolds with a cylindrical shape chitosan solutions were cast into silicone tubes. For the case of CHT1, the tubes with the crosslinked solution were maintained under stirring for 6h at 37 °C. Then, all solutions were frozen for 1 day at -80°C. After freeze-drying, the scaffolds were neutralized with a solution of NaOH (1M) and then freeze-dried again. The tubes were then cut in small pieces to obtain a scaffold dimension of 7 mm x Ø5 mm.

2.2.2 Scanning electron microscopy (SEM)

A NanoSEM FEI Nova 200 (FEG/SEM) scanning electron microscope was used to study the surface and the morphology of the samples. All samples were coated by gold sputtering for 2 minutes at a current of 15 mA, prior to observation.

2.2.3 Porosity measurements

The porosity of the scaffolds is obtained from the density of chitosan and the density of actual porous scaffolds sample produced. The density of chitosan (ρ) is 1.342 g/cm³. So the calculation formula of porosity is defined as:

$$porosity (\%) = \frac{V_m - (W_m/\rho)}{V_m} \times 100 \quad (1)$$

where, V_m is the total volume of chitosan scaffolds (cm³), and W_m is the mass of the scaffold (g).

2.2.4 Swelling of chitosan scaffolds in water/ethanol mixtures

The swelling of CHT scaffolds in mixtures of water/ethanol was determined by immersing previously weighted CHT scaffolds in mixtures of these solvents at compositions varying from pure water to pure ethanol at room temperature, for 4h hours. It was confirmed that after a 4h period the scaffolds had reached their swelling equilibrium. After 4h, swelled samples were blotted with filter paper to remove the adsorbed solvent and weighted immediately. The swelling ratio (S) was calculated using the following equation:

$$S(\text{wt. } \%) = \frac{(w-w_0)}{w_0} \times 100 \quad (2)$$

where, w is the swollen sample weight and w_0 is the dry sample weight. Each swelling experiment condition was performed in triplicate.

2.2.5 X-ray diffraction measurements

Crystallinity and phase content of chitosan scaffolds were investigated with X-ray diffraction (XRD) analysis, performed with a Bruker D8 Discover model. XRD patterns were examined in the region of 5–65° with a step size 0.02° for 2θ and a counting time of 2s step⁻¹.

2.2.6 Dynamic Mechanical Analysis (DMA)

Dynamical mechanical analysis was performed using a Tritec 2000B equipment (Triton Technology, UK). The measurements were carried out at room temperature (20°

C). Chitosan scaffolds were tested at constant frequency (1 Hz) following the changes in the storage modulus (E') and loss factor ($\tan \delta$) as function of the water content. The dried samples of known geometry were placed in a Teflon® reservoir and immersed in a defined volume of ethanol ($V_{eth} = 270$ ml) and kept under the testing constant strain amplitude (30 μm) during 30 min. After this step, E' reached an equilibrium value. Finally, the water was pumped into the reservoir at a constant flow rate ($Q = 14$ ml/min), providing a time (t) dependent change in the content of water described by the following equation:

$$water (vol. \%) = \frac{Qt}{Qt + V_{eth}} \quad (3)$$

In this measurements E' should be taken as an apparent value as during introduction of water the geometry of the sample continuously changes due to swelling and the calculation of this parameter used the initial geometry of the sample.

2.2.7 Hydromechanical Cyclic Compressive Tests

The compressive tests of the developed scaffolds were performed using a Universal tensile testing machine (Instron 4505 Universal Machine, USA). The tests were performed under compressive loading, by performing uniaxial compression, using a crosshead speed of 2 mm.min⁻¹, at a room temperature. The results presented are the average of at least three specimens. Each compressive test was performed with the scaffolds hydrated in water/ethanol mixtures with distinct compositions. Young's modulus (E) was determined from resulting stress/strain curves.

For the hydromechanical cyclic compressive tests, the samples were first hydrated and deformed up to different maximum strains ($\epsilon_m = 10, 20, 30$ and 60%). After the test and maintaining the strain, the stress was then held constant while the sample is dehydrated by immersing the sample in ethanol for 20 min, whereby the temporary shape is fixed. Then stress was completely removed to obtain the sample in its temporary shape, even after complete evaporation of ethanol. Finally, the samples were immersed in different mixtures of water/ethanol, varying from pure water to pure ethanol and the shape recovery was monitored.

In the hydromechanical cyclic compressive test, the shape memory capability of the SMP is typically characterized by the shape fixity ratio (R_f) and the shape recovery

ratio (R_f). R_f characterizes the ability of a system to fix its temporary shape and R_r is the recoverability of the permanent shape. R_f and R_r values can be calculated according to the following equations:

$$R_f(\%) = \frac{\epsilon_u}{\epsilon_m} \times 100 \quad (4)$$

$$R_r(\%) = 1 - \frac{\epsilon_p}{\epsilon_m} \times 100 \quad (5)$$

where ϵ_m is the applied maximum strain, ϵ_u is the fixed strain after unloading and ϵ_p , the permanent strain after induced recovery. The measures were performed with a digital micrometer (measurements were performed in triplicate).

The scaffolds recovery along time was evaluated to see how the hydrated scaffolds recovery after being submitted to compression loads. The scaffolds were initially hydrated and then compressed up to different maximum strains ($\epsilon_m = 10, 20$ and 30%). Then, the samples were dehydrated to fix the temporary shape. The samples were immersed again in water and their height was measured at different time points.

2.2.8 *In vitro* drug delivery studies

Congo Red (CR) was use as a model molecule to investigate the loading and release ability of the scaffold. CR is water soluble and presents a low solubility in ethanol³⁴.

In drug delivery studies it is important to know the incorporation efficiency (IE) of the scaffolds. The incorporation efficiency can be measured by the ratio of the drug available for release and the initial loaded drug,

$$IE = \frac{\text{drug available for release}}{\text{loaded drug}} \times 100 \quad (6)$$

The scaffold was immersed in a solution of CR in PBS of 1mg/ml for 1h. The loaded drug was estimated using the variation of the mass of the scaffold during the swelling. Then, the loaded scaffolds were compressed ($\epsilon_m=30\%$) and dehydrated follow by immersion in 5ml of PBS under sonication at 37°C for 5 days to induce a forced release, obtaining the maximum drug release. Such experiment permitted to estimate the total drug available for release in the scaffolds.

For the loading procedure, the samples were immersed in a solution of CR in PBS of 5mg/ml for a period of 1h. After complete hydration the samples were compressed ($\epsilon_m=30\%$) and dehydrated for 20min in ethanol, followed by the evaporation of the solvent. After the deformation and fixation of the temporary shape, both CHT0 and CHT1 were immersed in 5ml of PBS, pH 7.4. The vials containing the scaffolds were kept under agitation (at approximately 60 rpm) in a water bath at 37°C. At pre-established periods of time, aliquots of 1ml of the supernatant were taken out and replaced with equal volume of fresh PBS to maintain the volume constant during the release study. The amount of Congo red were quantified spectrophotometrically, measuring the UV absorbance at 498nm (Synergie HT, Bio-Tek, USA) and using a calibration curve generated by absorption measurements of CR solutions with pre-defined concentrations.

3. Results and Discussion

3.1 Morphological Characterization

Adequate scaffolds used for tissue engineering should typically exhibit a homogenous microstructure, suitable pore size distribution and high porosity. Such microstructure should act as an extracellular matrix analog, functioning as a necessary template for host infiltration and as a physical support to guide the differentiation and proliferation of cells into the targeted functional tissue or organ ³⁵.

The SEM images in Figure III.1 show the morphological characteristics of the non-crosslinked (CHT0) and crosslinked (CHT1) scaffolds at the microscale level. The scaffold revealed an interconnected porous structure, with pores sizes in the range of 200-350 μm for CHT0. CHT1 show a more regular morphology with smaller pore in the range of 100-250 μm . The pores walls in CHT1 are thinner and the amount of pores is higher; thus the overall surface area for possible cell attachment is larger for CHT1. The CHT0 and CHT1 scaffolds have a density of 0.15 g/cm^3 and 0.08 g/cm^3 , respectively. The decreased in the density of CHT1 result in a porosity of 94% higher than the 88% obtained for CHT0.

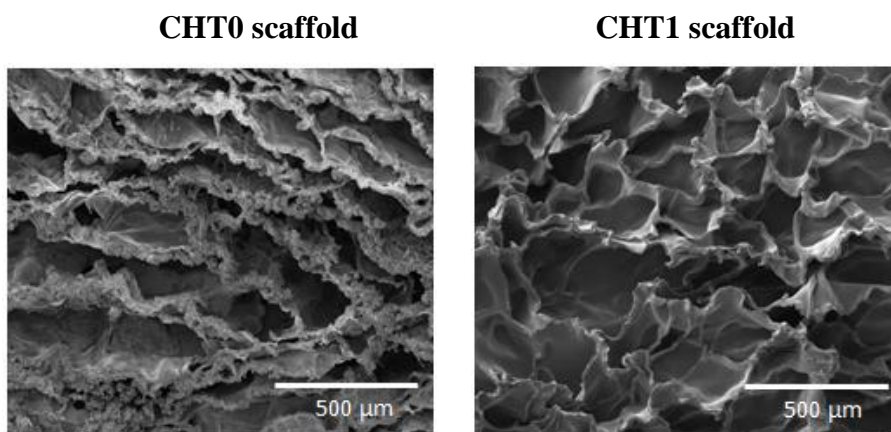


Figure III.1 - SEM images of porous non-crosslinked (CHT0) and crosslinked (CHT1) chitosan scaffolds.

3.2 Swelling of chitosan scaffolds in water/ethanol mixtures

In the presence of suitable solvents, chemically or physically crosslinked polymer networks do not dissolve, but absorb limited amounts of solvent swelling until the equilibrium is reached. The swelling test was used to evaluate the absorption capabilities of non-crosslinked (CHT0) and crosslinked (CHT1) chitosan scaffolds in mixtures of a non-solvent (ethanol) and a solvent (water) - see Figure III.2. The combined effect of solvent and non-solvent in miscible liquid pairs is expected to be rather useful to control the swelling ratio within polymer networks. CHT, which is a semi-crystalline polymer, absorbs considerable amounts of water when immersed in aqueous environments³⁶. Ethanol was used as a non-solvent, aiming at providing an adequate control over the CHT scaffolds swelling capability.

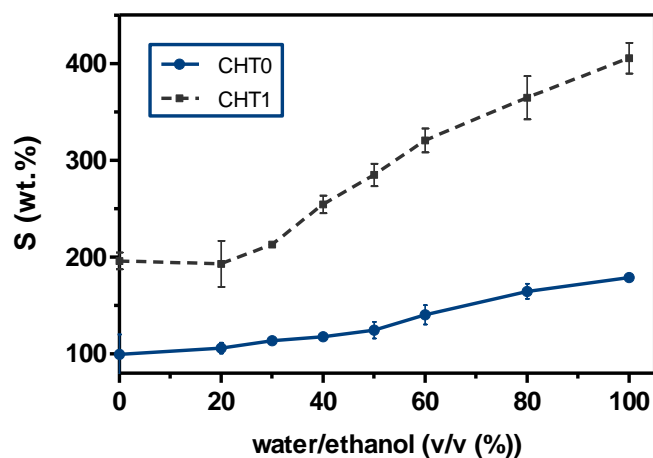


Figure III.2 - Swelling capability of non-crosslinked (CHT0) and crosslinked (CHT1) chitosan scaffolds determined after immersion in distinct water/ethanol mixtures.

With increasing water content, the swelling increases for both conditions. Below 30 vol.% for CHT1 and 50 vol.% for CHT0 such increase is not evident, but above such values the swelling starts to increase prominently in both cases. These results agree with those of Ilavsky et al., who described polymeric hydrophilic networks in which a small variation in the composition of water/ethanol mixtures induces a jumpwise change in the volume of the gel, which is reflected by a simultaneous jumpwise change in the shear modulus³⁷. They also found that in those types of systems the mechanical behavior was predominantly determined by the degree of swelling: the jumpwise change in the modulus adequately correlated with the jump in the swelling ratio. In the case under study, a jump in swelling ratio of the CHT scaffolds is a strong indication that the referred type of volume transition occur under the experimental conditions.

The swelling in the CHT scaffolds could be attributed to both of their moderate hydrophilicity and the presence of pores that can be filled with liquid. The swelling results show that CHT1 present higher solvent uptake capability than CHT0 in all water/ethanol compositions. The maximum swelling, reached for 100 vol.% of water, is 179 vol.% for CHT0 and for CH1 is more than double, 405%. For the case of pure ethanol the swelling is also about the double in CHT1 as compared to CHT0. The observed differences could be consequence of the different porous microstructure and also because genipin that was used to crosslink CHT1 exhibits a high affinity to both water and ethanol.

The effect of swelling was also observed in x-ray diffraction analysis of CHT0. Figure III.3, shows the diffraction patterns of the CHT0 scaffolds immersed in different mixtures of water/ethanol. A strong reflexion at $2\theta=19$ is observed for dehydrated chitosan (0% water) in the diffraction patterns for CHT0, which evidences the semi-crystalline nature of CHT. With the increasing of water content, the relative intensity of the reflection was significantly diminished. This is particularly evident above 50 vol.% where an amorphous halo centered at about $2\theta=28^\circ$ is very visible. This occurrence can be explained by the jumpwise of swelling for CHT0 observed at 50 vol.%, see Figure III.2. This increasing of solvent in the polymeric matrix hides the crystalline diffraction pattern of chitosan. Nevertheless, the semi-crystalline nature of CHT is maintained even upon immersion in pure water. The crystalline domains act as anchorage points for the amorphous fraction, being a necessary requirement for shape memory ability.

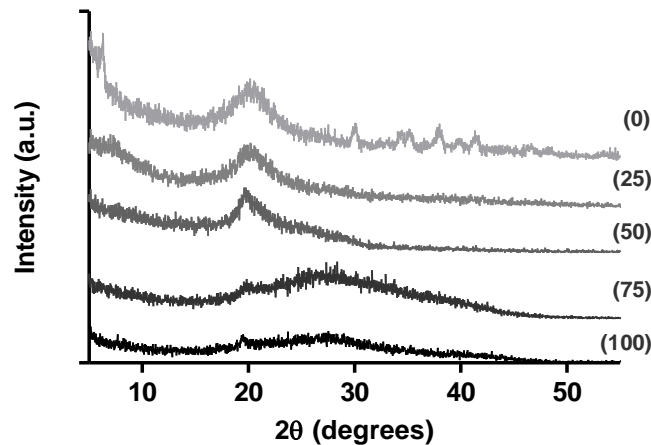


Figure III.3 - XRD pattern for CHT0 immersed in different mixtures of water/ethanol from 0% to 100% of water.

3.3 Dynamical mechanical analysis measurements

In biomedical applications, chitosan can be exposed to different levels of hydration, which can vary from moderate humidity levels to maximum values of water uptake capability, for example, in implantable conditions. The influence of water content on the viscoelastic properties of chitosan films was already study and was observed that chitosan can undergo a glass transition at room/body temperatures by the action of hydration ^{32,33}.

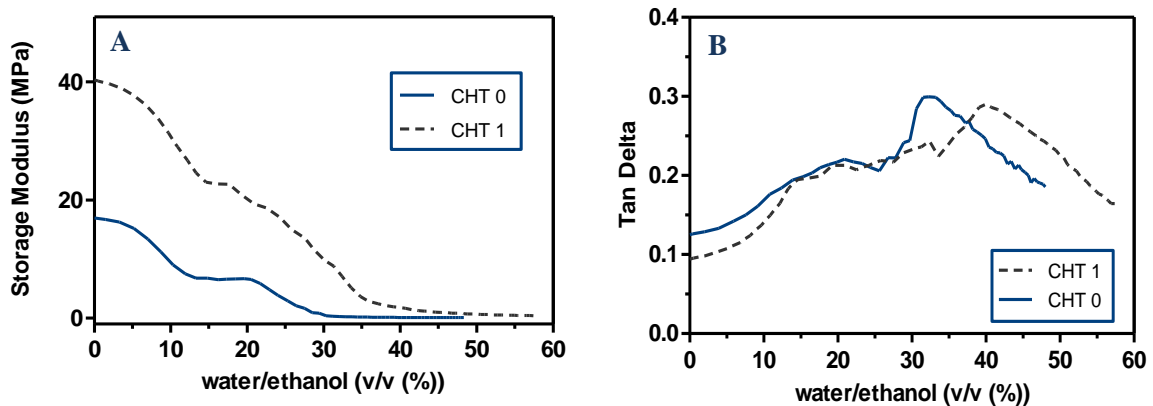


Figure III.4 - Apparent storage modulus (A) and loss factor (B) measured with samples immersed in water/ethanol mixtures for CHT0 and CHT1 at 1Hz.

Dynamic mechanical analysis, DMA, was used to determine the storage modulus (E') and loss factor ($\tan \delta$) of CHT0 and CHT1 scaffolds as a function of water content. The chitosan scaffolds were placed in the DMA apparatus and immersed in an ethanol solution. The DMA parameters were then continuously monitored at 1 Hz. During the measurements water was introduced in the reservoir at a constant flow rate, changing

gradually the composition of the mixture (equation 2). Figure III.4 shows the variation of the storage modulus and the loss factor as a function of the water composition in the liquid mixture of the bath. The storage modulus of both samples shows a decrease with the increase of water content, with a profile suggesting the occurrence of a relaxation process induced by enriching the water content in the chitosan structure. This decreasing of storage modules with increasing of water was also observed in chitosan membranes immersed in mixtures of water/ethanol³³. The samples show a plateau storage modulus at water content of above 28.5 vol.% for CHT0 and 39.1 vol.% for CHT1. In the dehydrated state CHT1 exhibits the highest storage modulus of ca 40 MPa in comparison with ca 17 MPa of CHT0. With increasing water content the $\tan \delta$ curve of the samples exhibits a broad relaxation process that seems to be characterized by two components. Dielectric relaxation experiments performed at different temperatures and frequencies pointed out for the complex relaxation pattern of chitosan³⁸⁻⁴⁰. However, the segmental mobility was never accessed before by this technique at different hydration levels.

The first component of the relaxation process that occurred in the range from 17 vol.% to 25 vol.% with a peak maximum around 21 vol.% is attributed to the glass transition of the fraction of amorphous domains, that need lower water content to transit to the rubbery state. The component of the relaxation process taking place at higher water content appears as a pronounced peak that reflects the glass transition of the amorphous domains confined in more restricted regions that are influenced by hard domains (crystalline and crosslinked environments). The occurrence of two glass transitions can be observed in semi-crystalline polymers reflecting molecular mobility of the amorphous chains in the non-confined bulk and segments with restricted mobility. Due to geometrical confinements generated by crystalline structures⁴¹. For CHT0 the peak is seen at ca 32 vol.% of water and for CHT1 is at 40 vol.%. Above such water contents, i.e. above glass transition, the storage modulus is almost constant and the rubbery state of the polymeric structure is obtained. It is possible to see that CHT1 has a peak shifted towards higher water contents, indicating that the glass transition takes place for an increases of approximately 10 vol.% of water. This could be explained by the effect of crosslinking that influences the dynamics (slowing down) of the segmental motions⁴².

3.4 Shape memory behavior of chitosan

Several authors proposed the use of SMP to fabricate fillers for pathological defects reparation to permit the implantation using less invasive procedures and to maximize the geometrical adaptation of the material in the defect cavity^{9,43}. The interest in this type of materials arises from the fact that SMPs can be deformed from a temporary shape into a stable secondary shape, significantly smaller than the primary. Therefore, evaluation of the shape recovery ability, in terms of final recovery, recovery rates and fixating ability is hence mandatory.

The first test performed to study the shape memory effect of chitosan scaffolds was the water-driven recovery. The hydrated CHT0 was compressed under different maximum strains (ϵ_m) and retained this strain during dehydration to fix the temporary shape. After immersing the sample in water at room temperature, it started immediately to recover. The results, as shown in Figure III.5, demonstrate that the recovery occurs essentially in the first 5 min for the different ϵ_m . After approximately 15 minutes, the samples have already achieved the final shape. The increasing of the maximum strain leads to a small decreasing of the recovery ratio.

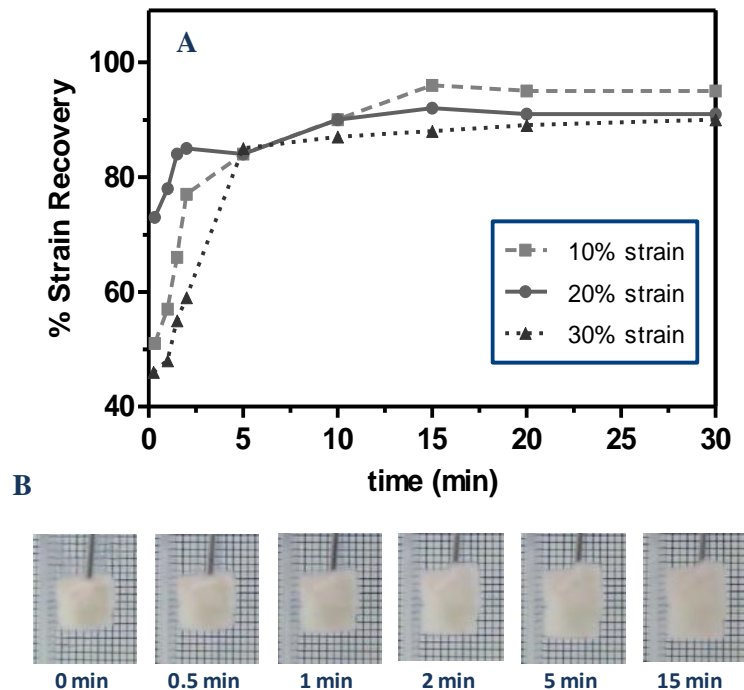


Figure III.5 - CHT0 shape recovery along time after different maximum strains (ϵ_m) (A). Series of photographs demonstrating the shape recovery process for CHT0; the referred times indicate the immersion time in water upon deformation at $\epsilon_m=30\%$ and dehydration (B).

The influence of the applied ϵ_m on the shape memory performance of CHT scaffolds was investigated by hydromechanical tests with $\epsilon_m = 10, 20, 30, 60\%$. The strain fixity R_f and the strain recovery R_r were calculated to quantify the fixation of the temporary shape and the recovery of the permanent shape of the polymer networks. Both CHT0 and CHT1 scaffolds exhibited excellent shape memory properties as summarized in Table III.1. A fixation of the deformation with $R_f \geq 97.2\%$ was obtained for CHT0 and an almost complete fixation with $R_f \geq 99.2\%$ was observed for CHT1, while the recovery of the original shape occurred with high R_r values: 70.5% for CHT0 and 98.5% for CHT1.

The recovery ratio increased with decreasing maximum strain. Too high deformation amplitude would render the shape memory effect more unsatisfied for CHT0. Such effect is not seen in CHT1. This result indicates that the crystalline structure in chitosan which affords all the shape recovery force in CHT0 may be not completely effective for large deformation strains. However, the crosslinking with genipin provides extra-anchorage points enhancing the recovery capability of the structure to the permanent shape.

Table III.2 - Shape memory properties of CHT0 and CHT1 at different deformation strains (ϵ_m)

	ϵ_m	Strain Fixity (R_f) (%)	Strain Recovery (R_r) (%)
CHT0	10%	98.4 ± 4.2	96.8 ± 3.6
	20%	97.7 ± 2.9	91.8 ± 1.5
	30%	97.2 ± 1.9	87.5 ± 2.8
	60%	98.8 ± 0.2	70.5 ± 5.5
CHT1	10%	100 ± 0.6	100 ± 0.8
	20%	99.8 ± 1.0	99.1 ± 2.3
	30%	99.2 ± 0.5	98.5 ± 1.7
	60%	99 ± 1.9	98.7 ± 1.2

Figure III.6A shows the variation of strain recovery along hydration in CHT0 for different deformation strains. The scaffold don't exhibit significant strain recovery for water content below 25 vol.%. The strain recovery starts between 25 and 50 vol. % having a drastically increase in the range of 50-75 vol.%, mainly for 20 and 30% strain. Such results are consistent with the swelling results in Figure III.2 and the occurrence of glass transition as seen by DMA (Figure III.4). As mentioned before, the strain recovery ratio decreased with increasing of maximum strain and for 60% strain the recovery is

unsatisfied for CHT0 that did not reached the permanent shape upon fully hydration. Therefore, in the following studies of the shape memory effect of CHT scaffolds, the maximum deformation strain was set as 30%. However, crosslinked CHT present better mechanical properties, and an excellent recoverability (Table III.1 and Figure III.6B).

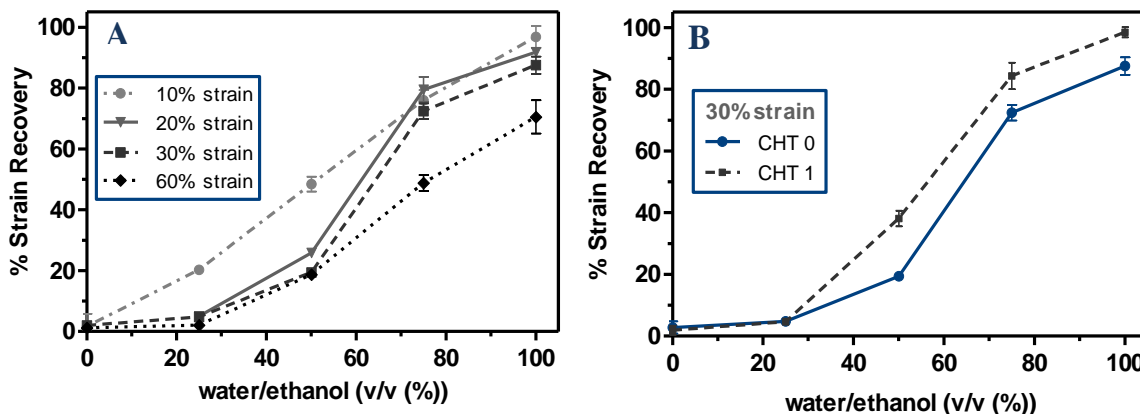


Figure III.6 - A - Strain recovery of CHT0 in different mixtures of water/ethanol after different ϵ_m . B - Strain recovery of CHT0 and CHT1 for $\epsilon_m=30\%$.

3.5 Young's modulus of the scaffolds at distinct hydration levels

The Young's modulus (E) of the developed scaffolds upon immersion in water/ethanol mixtures was assessed via uniaxial compressive tests, obtained from the slope of the stress-strain curve. Figure III.7 shows an inverse relationship between E versus water content of the liquid. Water acts as a very good plasticizer even in small quantities. In the presence of water, the interference between water and the chain-to-chain secondary bonding reduces the intermolecular forces. As a result, chains acquire greater mobility and the free volume increases, leading to a decrease in the glass transition and stiffness⁴⁴. Such process is in the origin of the occurrence of the glass transition of the system as discussed before. Increasing plasticizer content resulted in scaffolds with lower E and then more flexible.

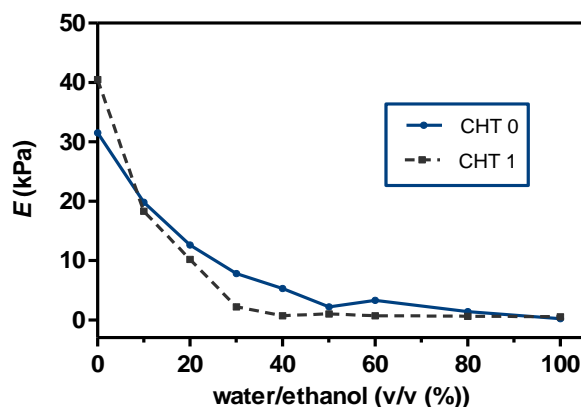


Figure III.7 - The variation of Young's Modulus with water/ethanol mixtures for CHT0 and CHT1.

For both scaffolds, CHT0 and CHT1, as the water content increased, E systematically decreased. The scaffolds exhibited water-dependent Young's modulus from 40.5 to 0.2 kPa. The values obtained for the scaffolds dehydrated are in accordance with the values obtained in previously reports for chitosan scaffolds in dry state⁴⁵. With the decrease of water content, the increasing of E starts, in the vicinity of the glass transition event, for water contents below approximately 40%. For water contents above 40% all the samples show a plateau in the modulus, suggesting a rubber like structure where the mobile chains in the amorphous regions are sustained by the crystalline and crosslinked domains.

3.6 Hydromechanical compressive cycle

To obtain more detailed shape memory properties of crosslinked and un-crosslinked CHT scaffolds, hydromechanical cyclic compressive tests were performed. The ensemble of the three-dimensional stress–strain–hydration response of the studied CHT0 and CHT1 shape memory scaffolds under uniaxial loading is shown in Figure III.8. The cycle starts hydrating the scaffold to reach humidity above the glass transition followed by a compression at a constant strain rate, resulting in a continuous stress-strain curve (curve I in Figure III.8). Afterwards the temporary shape is fixed by dehydrating the scaffolds at constant compression ($\epsilon_m=30\%$) (stage II in Figure III.8). Then, the compressive stress is reduced until a stress-free condition is reached (stage III in Figure III.8). The scaffold is finally hydrated while the compressive stress is kept constant at 0 kPa (sequence IV in Figure III.8). Such process was performed by immersing the scaffolds in water/ethanol mixtures with increasing water content. The permanent shape is recovered while passing the glass transition, resulting in the strain-water content relationship.

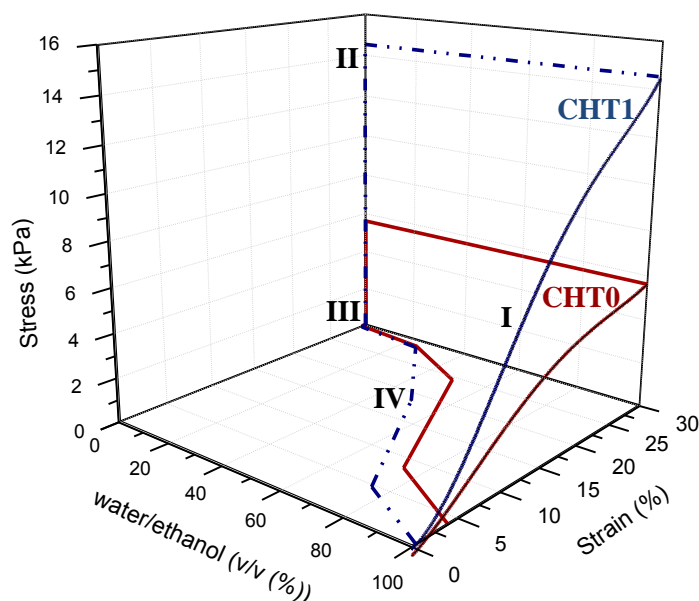


Figure III.8 - Hydromechanical compressive cycle of CHT and CHT/BG-NPs. I: compression at a constant rate of the hydrated sample; II - dehydration of the sample at a fixed strain; III - release of the stress; IV - hydration in water/ethanol mixtures with increase content in water.

The stress-strain curves were performed for CHT0 and CHT1 in hydrated conditions by compression tests up to $\epsilon_m = 30\%$. The scaffolds exhibited the typical response observed in soft cellular materials for relatively low deformations. Compared to CHT0 scaffolds, CHT1 achieves a higher compressive stress at $\epsilon_m=30\%$ and the slope of the initial straight line is also higher than CHT0, confirming that CHT1 has a higher compressive modulus (E). After loading, ϵ_m is maintained while the samples are dehydrated. When the stress is removed the scaffolds reach the temporary shape.

The strain-hydration curves present in the compressive cycle were obtained by hydration of the dehydrated scaffolds in mixtures of water and ethanol, varying from pure ethanol to pure water. As can be seen, in the hydration process, the strain is recovered significantly above 40% of water content, for water content rate above the glass transition occurrence.

3.7 *In vitro* drug delivery studies

The potentiality of the system for loaded and *in-situ* release drugs were explored in order to achieve a multifunctional polymer system that combines SME, biodegradability and controlled drug release. In this study, Congo Red was selected as a model molecule and was loaded in the scaffolds by swelling. CR is water soluble and presents a low solubility in ethanol. The swelling of the scaffolds in CR solutions at room temperature permits the introduction of CR in the polymer matrix. With this

technique the loading is dependent of the CR concentration and the swelling of the polymer network in the solution. After loading, the scaffolds were compressed and dehydrated under stress to achieve the temporary shape. Then, the release studies with CHT0 and CHT1 loaded with CR were conducted at 37°C in PBS. Figure III.9A present the release profiles for CHT0 and CHT1, during 48h. For both scaffolds, the CR was released relatively quickly up to 2 hours and then the release rate slowed with time. The initial fast release observed in both profiles can be attributed to the presence of the CR on (or close to) the scaffold's surface. The ability of the scaffolds to swell leads to the increase of the pore size in the scaffold structure that allows the diffusion of the CR to the PBS solution. Thus, as the CHT1 present better water uptake capability it also release more CR than CHT0.

We envisage the possibility of using such technology to deliver therapeutic drugs in specific sites in the body. As an exemplification we used gelatin as a continuous medium simulating a soft tissue. A defect in a gelatin block was produced with a size between the permanent and temporary sizes of the scaffolds. The scaffolds containing CR were placed in the region of the empty space. Figure III.9B shows an image of the system after the introduction of the scaffold and after 8h of release. After this period of time it is possible to see a gradient with higher concentration of CR next to the scaffolds, indicating a diffusion of the molecule to the medium. This result reveals that the developed shape memory device can be potentially use as a drug loading matrix. Moreover it could be also observed that upon recovery in the hydrated state the scaffold was able to accommodate perfectly in the entire geometry of the defect site and could be maintained tightly in this volume due to a press fitting effect.

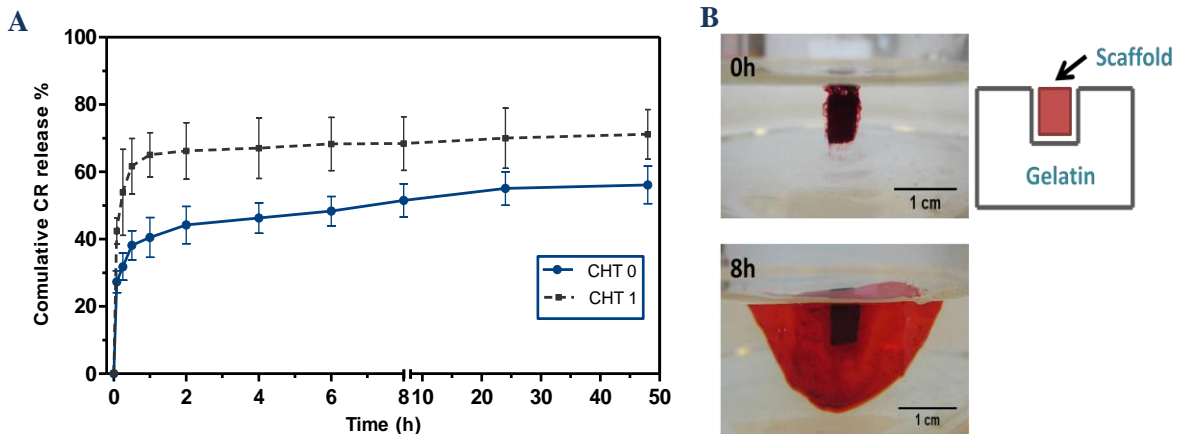


Figure III.9 - A - *In vitro* release of CR as a function of time for CHT0 and CHT1 in PBS (37°C). B - Images showing CR being release from a CHT0 scaffold after being placed in a defect produced in a gelatin block.

4. Conclusions

Semi-crystalline (CHT0) and chemically crosslinked (CHT1) crosslinked CHT scaffolds, showed shape memory effect using hydration as the stimuli. CHT0 exhibit the occurrence of a glass transition for 32.3 vol.% of water in water/ethanol mixtures and CHT1 at 40 vol.%. Both scaffolds possess good shape memory properties, fixity ratio above 97.2% for CHT0 and above 99.2% for CHT1 and a recovery ratio above 70.5% for CHT0 and 98.5% for CHT1. The shape memory properties decreased with increasing maximum deformation. However, CHT1 present better mechanical properties, and an excellent recoverability even for high deformations. The release profiles of CR from the scaffolds show that the developed porous structures could be used as a controlled delivery system. We can conclude that the CHT scaffolds proposed in this work are candidates for applications in minimally invasive surgery with multifunctional characteristics, combining biodegradability, shape-memory capability and controlled drug release.

5. Acknowledgments

This work was supported by the Portuguese Foundation for Science and Technology Foundation (FCT) through project PTDC/FIS/115048/2009. We acknowledge Dr. Ana Rita Duarte for all the help during this project and Joana Marques Silva and Sofia Caridade for their contribution to the DMA experiments.

6. References

- 1 Wischke, C., Neffe, A. T. & Lendlein, A. in *Shape-Memory Polymers* 177-205 (Springer, 2010).
- 2 Behl, M., Razzaq, M. Y. & Lendlein, A. Multifunctional Shape-Memory Polymers. *Advanced Materials* **22**, 3388-3410 (2010).
- 3 Serrano, M. C. & Ameer, G. A. Recent Insights Into the Biomedical Applications of Shape-memory Polymers. *Macromolecular bioscience* **12**, 1156-1171 (2012).
- 4 Lendlein, A. *Shape-Memory Polymers*. Vol. 226 (Springer, 2009).
- 5 Liu, F. & Urban, M. W. Recent advances and challenges in designing stimuli-responsive polymers. *Progress in Polymer Science* **35**, 3-23 (2010).
- 6 Rousseau, I. A. Challenges of shape memory polymers: A review of the progress toward overcoming SMP's limitations. *Polymer Engineering & Science* **48**, 2075-2089 (2008).
- 7 Choi, N.-y. & Lendlein, A. Degradable shape-memory polymer networks from oligo [(L-lactide)-ran-glycolide] dimethacrylates. *Soft Matter* **3**, 901-909 (2007).

-
- 8 Yang, B., Min Huang, W., Li, C. & Hoe Chor, J. Effects of moisture on the glass transition temperature of polyurethane shape memory polymer filled with nano-carbon powder. *European polymer journal* **41**, 1123-1128 (2005).
- 9 Lendlein, A. & Kelch, S. Shape-memory polymers. *Angewandte Chemie International Edition* **41**, 2034-2057 (2002).
- 10 Ghobadi, E., Heuchel, M., Kratz, K. & Lendlein, A. Influence of the addition of water to amorphous switching domains on the simulated shape-memory properties of poly (L-lactide). *Polymer* (2013).
- 11 Lendlein, A., Jiang, H., Jünger, O. & Langer, R. Light-induced shape-memory polymers. *Nature* **434**, 879-882 (2005).
- 12 Weigel, T., Mohr, R. & Lendlein, A. Investigation of parameters to achieve temperatures required to initiate the shape-memory effect of magnetic nanocomposites by inductive heating. *Smart Materials and Structures* **18**, 025011 (2009).
- 13 Cho, J. W., Kim, J. W., Jung, Y. C. & Goo, N. S. Electroactive shape-memory polyurethane composites incorporating carbon nanotubes. *Macromolecular Rapid Communications* **26**, 412-416 (2005).
- 14 Zhang, H., Wang, H., Zhong, W. & Du, Q. A novel type of shape memory polymer blend and the shape memory mechanism. *Polymer* **50**, 1596-1601 (2009).
- 15 Chen, S., Hu, J. & Chen, S. Studies of the moisture-sensitive shape memory effect of pyridine-containing polyurethanes. *Polymer International* **61**, 314-320 (2012).
- 16 Niu, G. & Cohn, D. Water Triggered Shape Memory Materials. *Science* **3**, 49-50 (2013).
- 17 Huang, W., Yang, B., Zhao, Y. & Ding, Z. Thermo-moisture responsive polyurethane shape-memory polymer and composites: a review. *Journal of Materials Chemistry* **20**, 3367-3381 (2010).
- 18 Du, H. & Zhang, J. Solvent induced shape recovery of shape memory polymer based on chemically cross-linked poly (vinyl alcohol). *Soft Matter* **6**, 3370-3376 (2010).
- 19 Fan, K. *et al.* Water-responsive shape memory hybrid: design concept and demonstration. *Express Polymer Letters* **5**, 409-416 (2011).
- 20 Wang, C. C., Huang, W. M., Ding, Z., Zhao, Y. & Purnawali, H. Cooling-/water-responsive shape memory hybrids. *Composites Science and Technology* **72**, 1178-1182 (2012).
- 21 Yang, B., Huang, W., Li, C., Lee, C. & Li, L. On the effects of moisture in a polyurethane shape memory polymer. *Smart Materials and Structures* **13**, 191 (2004).
- 22 Pierce, B. F., Bellin, K., Behl, M. & Lendlein, A. Demonstrating the influence of water on shape-memory polymer networks based on poly [(rac-lactide)-co-glycolide] segments in vitro. *International journal of artificial organs* **34**, 172-179 (2011).
- 23 Lv, H., Leng, J., Liu, Y. & Du, S. Shape-Memory Polymer in Response to Solution. *Advanced Engineering Materials* **10**, 592-595 (2008).
- 24 De Nardo, L., Farè, S., Cicco, S. D., Jovenitti, M. & Tanzi, M. C. in *Materials science forum*. 663-668 (Trans Tech Publ).
- 25 Wong, Y., Xiong, Y., Venkatraman, S. & Boey, F. Shape memory in un-cross-linked biodegradable polymers. *Journal of Biomaterials Science, Polymer Edition* **19**, 175-191 (2008).
- 26 Bao, M., Zhou, Q., Dong, W., Lou, X. & Zhang, Y. Ultrasound-modulated shape memory and payload release effects in a biodegradable cylindrical rod made of chitosan-functionalized PLGA microspheres. *Biomacromolecules* (2013).

-
- 27 Alves, N. & Mano, J. Chitosan derivatives obtained by chemical modifications for biomedical and environmental applications. *International Journal of Biological Macromolecules* **43**, 401-414 (2008).
- 28 VandeVord, P. J. *et al.* Evaluation of the biocompatibility of a chitosan scaffold in mice. *Journal of biomedical materials research* **59**, 585-590 (2002).
- 29 Kim, I.-Y. *et al.* Chitosan and its derivatives for tissue engineering applications. *Biotechnology Advances* **26**, 1-21 (2008).
- 30 Di Martino, A., Sittinger, M. & Risbud, M. V. Chitosan: a versatile biopolymer for orthopaedic tissue-engineering. *Biomaterials* **26**, 5983-5990 (2005).
- 31 Mano, J. *et al.* Natural origin biodegradable systems in tissue engineering and regenerative medicine: present status and some moving trends. *Journal of the Royal Society Interface* **4**, 999-1030 (2007).
- 32 Mano, J. F. Viscoelastic properties of chitosan with different hydration degrees as studied by dynamic mechanical analysis. *Macromolecular bioscience* **8**, 69-76 (2008).
- 33 Caridade, S. G., da Silva, R. M., Reis, R. L. & Mano, J. F. Effect of solvent-dependent viscoelastic properties of chitosan membranes on the permeation of 2-phenylethanol. *Carbohydrate Polymers* **75**, 651-659 (2009).
- 34 Teather, R. M. & Wood, P. J. Use of Congo red-polysaccharide interactions in enumeration and characterization of cellulolytic bacteria from the bovine rumen. *Applied and environmental microbiology* **43**, 777-780 (1982).
- 35 Ma, L. *et al.* Collagen/chitosan porous scaffolds with improved biostability for skin tissue engineering. *Biomaterials* **24**, 4833-4841 (2003).
- 36 Silva, R., Silva, G., Coutinho, O., Mano, J. & Reis, R. Preparation and characterisation in simulated body conditions of glutaraldehyde crosslinked chitosan membranes. *Journal of Materials Science: Materials in Medicine* **15**, 1105-1112 (2004).
- 37 Ilavsky, M. Phase transition in swollen gels. 2. Effect of charge concentration on the collapse and mechanical behavior of polyacrylamide networks. *Macromolecules* **15**, 782-788 (1982).
- 38 Viciosa, M., Dionísio, M., Silva, R., Reis, R. & Mano, J. Molecular motions in chitosan studied by dielectric relaxation spectroscopy. *Biomacromolecules* **5**, 2073-2078 (2004).
- 39 Viciosa, M., Dionísio, M. & Mano, J. Dielectric characterization of neutralized and nonneutralized chitosan upon drying. *Biopolymers* **81**, 149-159 (2006).
- 40 Gartner, C. *et al.* Interplay between structure and dynamics in chitosan films investigated with solid-state NMR, dynamic mechanical analysis, and X-ray diffraction. *Biomacromolecules* **12**, 1380-1386 (2011).
- 41 Wang, Y., Gómez Ribelles, J., Salmerón Sánchez, M. & Mano, J. Morphological contributions to glass transition in poly (l-lactic acid). *Macromolecules* **38**, 4712-4718 (2005).
- 42 Alves, N., Ribelles, G., Tejedor, G. & Mano, J. Viscoelastic behavior of poly (methyl methacrylate) networks with different cross-linking degrees. *Macromolecules* **37**, 3735-3744 (2004).
- 43 Lendlein, A., Behl, M., Hiebl, B. & Wischke, C. Shape-memory polymers as a technology platform for biomedical applications. *Expert review of medical devices* **7**, 357-379 (2010).
- 44 Yang, B., Huang, W., Li, C. & Li, L. Effects of moisture on the thermomechanical properties of a polyurethane shape memory polymer. *Polymer* **47**, 1348-1356 (2006).
-

-
- 45 Liu, M., Wu, C., Jiao, Y., Xiong, S. & Zhou, C. Chitosan–halloysite nanotubes nanocomposite scaffolds for tissue engineering. *J. Mater. Chem. B* **1**, 2078-2089 (2013).

**Chapter IV.- Chitosan/Bioactive Glass Nanoparticles Scaffolds with
Shape Memory Properties**

Chitosan/Bioactive Glass Nanoparticles Scaffolds with Shape Memory Properties

Cristina O. Correia.^{1,2}, Álvaro J. Leite, M.Sc.^{1,2}, and João F. Mano, Ph.D.^{1,2}.

1 3B's Research Group – Biomaterials, Biodegradables and Biomimetics; Department of Polymer Engineering, University of Minho; Headquarters of the European Institute of Excellence on Tissue Engineering and Regenerative Medicine; AvePark, Zona Industrial da Gandra S. Cláudio do Barco, 4806-909 Caldas das Taipas, Guimarães, Portugal

2 ICVS/3B's, PT Government Associate Laboratory, Braga/Guimarães, Portugal

Abstract

We propose a combination of chitosan (CHT) with bioactive glass nanoparticles (BG-NPs) in order to produce CHT/BG-NPs scaffolds that combined the shape memory properties of chitosan and the biomineralization ability of BG-NPs for applications in bone regeneration. The addition of BG-NPs to the CHT polymeric matrix improved the mechanical properties and the bioactivity of the composite scaffold, as seen by the precipitation of bone-like apatite layer upon immersion in simulated body fluid (SBF). Shape memory tests were carried out while the samples were immersed in varying compositions of water/ethanol mixtures. Dehydration with ethanol enables to fix a temporary shape of a deformed scaffold that recovers the initial geometry upon water uptake. The scaffolds present good shape memory properties characterized by a recovery ratio of 87.5% for CHT and 89.9% for CHT/BG-NPs and a fixity ratio of was 97.2% for CHT and 98.2% for CHT/BG-NPs (for 30% compressive deformation). The applicability of such structures was demonstrated by a good geometrical accommodation of a previously compressed scaffold in a bone defect. The results indicate that the developed CHT/BG-NPs scaffolds are candidate for applications in bone tissue engineering.

Keywords: Bioactive glass nanoparticles, chitosan, shape memory, bioactivity.

1. Introduction

Shape memory polymers (SMPs) represent a technologically important class of stimuli-responsive materials that offer mechanical and geometrical action triggered by an external stimulus. SMP can be deformed and subsequently fixed into a temporary shape, which would remain stable unless it is exposed to an appropriate external stimulus that triggers the polymer to recover its original shape ¹. This advanced functionality makes SMP suitable and promising materials for diverse technological applications, including the fabrication of smart biomedical devices.

Although SMP materials have found a niche application as an actuation material in biomedical applications, they have not fully reached their technological potential. A significant drawback of unreinforced SMP materials is their low stiffness and strength compared to alloys or ceramics ². The relatively low recovery stress becomes a limiting factor in many applications especially in cases where SMP devices should overcome a large resisting stress during shape recovery. Thus incorporation of reinforcing elements has been investigated in order to improve the mechanical properties and to diversify the applications of SMPs. Incorporation of filler leads to an improvement in material properties, such as modulus, strength, stiffness and heat resistance ^{3,4}. The enhancement of material properties and creation of novel functions has been linked to the interfacial interaction between the polymer matrix and fillers as well the formation of a network of interconnected filler particles ⁵.

Among the naturally occurring polymers which can be used as such as smart polymers, polysaccharides constitutes a very common and important family of biomolecules ⁶. Between them, Chitosan (CHT) is one of the most widely-used natural polymers in tissue engineering research, essentially because of their unique properties, such as biocompatibility, biodegradability, antibacterial activity, wound healing properties and easy accessibility ^{7,8}. Previous studies showed that CHT can undergo a glass transition by the action of hydration ^{9,10}. Therefore, we hypothesis that the occurrence of a glass transition in chitosan activated by hydration variation could be used in the production of devices with shape memory capability, that could find interest in the biomedical field. Chitosan is a biocompatible polymer, although, by itself, it is not capable of reacting within the physiological fluid in order to develop apatite crystals and bond to the bone. To improve the bioactivity of CHT it is necessary to combine it with other bioactive materials ^{11,12}. Bioactive glasses are well suited materials to be

incorporated with polymers for bone tissue regeneration due to their chemical interaction with surrounding bone tissue *in vivo*, which promotes osteointegration by the formation of a calcium phosphate layer which is later modified by bone cells^{13,14}. Moreover, the ionic release from bioactive glasses may stimulate gene expression, promoting osteoinduction, and in a nanoparticulate form they can be combined with polymeric materials to produce bioactive nanocomposites^{15,16}.

This work presents the development of bioactive composites using bioactive glass nanoparticles (BG-NPs) prepared via a sol-gel route as a filler in the CHT scaffolds to combine the advantages of the polymeric and the inorganic components¹³. The use of bioactive particles can improve bioactivity, the remineralisation and mechanical properties of CHT. Thus, we hypothesize that combining the mineralization induced by the BG-NPs with the shape memory capability of the CHT we can create a multifunctional polymer with potential applications in bone tissue engineering and other orthopedic applications.

2. Materials and Methods

2.1 Materials

Chitosan (CHT) of medium molecular weight ($M_w = 190.000-310.000$, 75-85% Degree of deacetylation, viscosity 200-800 cps) was purchased from Sigma Aldrich. Tetraethyl orthosilicate (TEO) (99.90% pure), ammonium phosphate dibasic, calcium nitrate tetrahydrate (99%), citric acid monohydrate (99–100%), ammonium hydroxide (maximum 33% NH_3), poly(ethylene glycol) and all chemicals for SBF preparation were purchased from Sigma–Aldrich. All other chemicals were reagent grade and were used as received.

2.2 Methods

2.2.1 Bioglass nanoparticles (BG-NPs) preparation

To prepare the BG-NPs a protocol based on previous work was followed^{17,18}. The procedure for preparation of the ternary form of BG-NPs, composed by $\text{SiO}_2:\text{CaO}:\text{P}_2\text{O}_5$ (mol%) = 55:40:5, consisted in sequential reagent dissolutions that resulted in hydrolysis and polycondensation reactions. Tetraethyl orthosilicate (TEOS,

99.90% pure) was used as the Si precursor, ammonium hydrogen phosphate as the P precursor, calcium nitrate tetrahydrate (99%) as the Ca precursor, citric acid monohydrate (99-100%) to promote hydrolysis, absolute ethanol, ammonium hydroxide (maximum of 33% NH₃) as the jellyfying agent and polyethylene glycol 20 000 (PEG) as the surfactant. The mixture of precursor's solutions (7.639 g of calcium nitrate in 120 ml of distilled water, 9.167 g of TEOS in 60 ml of ethanol/ 30 ml of citric acid 10% (w/v)) was added drop-by-drop to an aqueous solution containing the phosphorous precursor (1.078 g of ammonium hydrogen phosphate in 1500 ml of distilled water). The pH was adjusted at 11.5 with ammonium hydroxide addition. The precipitate obtained was stirred for 48h, followed by a resting period of 24h. The precipitate was washed three times with distilled water. A 200 ml amount of an aqueous solution of poly(ethylene glycol) 2% (w/v) with M_w of 20000 was added to the precipitate, followed by freeze drying. Finally, the gel powder was calcinated at 700 °C for 5h to get the white bioactive glass nanoparticles.

2.2.2 Scaffolds Preparation

The scaffolds were obtained by freeze-drying. Chitosan was dissolved in an aqueous acetic acid solution 2% (v/v) to a concentration of 3% (w/v) for preparation of the control scaffold of pure chitosan, labeled CHT. The composite scaffold, labeled CHT/BG-NPs, were obtained by dissolving CHT (0.7 %wt) and BG-NPs (0.3 %wt) in the acetic acid solution. In order to obtain a cylindrical shape, both solutions were cast into silicone tubes and frozen for 1 day at -80°C. After freeze-drying, the scaffolds, were neutralized with a solution of NaOH (1M) and then freeze-dried again. The tubes were then cut in small pieces to obtain scaffolds with a dimension of 7mm x Ø5 mm.

2.2.3 *In vitro* bioactivity study

In vitro bioactivity tests were carried out by soaking single CHT/BG-NPs scaffolds in 20 ml of SBF for 3 and 7 days at 37°C. Upon removing from SBF the samples were rinsed with distilled water and left to dry. The preparation of SBF followed the protocol described by Kokubo and Takadama ¹⁹.

2.2.4 Scanning Electron Microscopy (SEM) and Energy Dispersive Spectroscopy (EDS)

To study the composition and morphology of the surfaces, a NanoSEM-Fei Nova 200 (FEG/SEM) scanning electron microscope was used. A Pegasus X4M instrument was used to perform EDS experiments.

2.2.5 Fourier-Transformed Infrared (FTIR) spectroscopy analysis

FTIR analyses were applied to study the composition of the scaffolds. The infrared spectrum was measured using a FTIR Spectrometer (model IRPrestige-21, Shimadzu; Germany) in the wavelength range of 4400–400 cm^{-1} . The samples were combined with potassium bromide (KBr) to produce discs.

2.2.6 Swelling of scaffolds in water/ethanol mixtures

The swelling of CHT and CHT/BG-NPS scaffolds in mixtures of ethanol/water was determined by immersing previously weighted chitosan scaffolds in mixtures of these solvents at compositions varying from pure water to pure ethanol at room temperature, for 4h hours. It was confirmed that after a 4h period the scaffolds had reached their swelling equilibrium. After 4h, swelled samples were blotted with filter paper to remove the adsorbed solvent and weighted immediately. The swelling ratio (S) was calculated using the following equation:

$$S(\text{wt. \%}) = \frac{(w-w_0)}{w_0} \times 100 \quad (1)$$

where, w is the swollen sample weight and w_0 is the dry sample weight. Each swelling experiment condition was performed in triplicate.

2.2.7 Hydromechanical Cyclic Compressive Tests

The compressive tests of the developed scaffolds were performed using a Universal tensile testing machine (Instron 4505 Universal Machine, USA). The tests were performed under compressive loading, by performing uniaxial compression, using a crosshead speed of 2 $\text{mm}\cdot\text{min}^{-1}$, at a room temperature. The results presented are the average of at least three specimens. The compressive test was performed with the scaffolds hydrated. After the test and maintaining the strain, the stress was then held

constant while the sample is dehydrated by immersing the sample in ethanol for 20 min, whereby the temporary shape is fixed. Then stress is completely removed and the sample is now in its temporary shape, even after complete evaporation of ethanol. Finally, the samples were immersed in different mixtures of water/ethanol, varying from pure water to pure ethanol and the shape memory effect is observed. The tests were performed for a maximum strain (ϵ_m) of 30%. Young's modulus (E) was determined from resulting stress/strain curves.

In a cyclic hydromechanical compressive test, the shape memory capability of a SMP is typically characterized by the shape fixity ratio (R_f) and the shape recovery ratio (R_r). R_f characterizes the ability of a system to fix its temporary shape and R_r is the recoverability of the permanent shape. R_f and R_r values can be calculated according to the following equations:

$$R_f(\%) = \frac{\epsilon_u}{\epsilon_m} \times 100 \quad (2)$$

$$R_r(\%) = 1 - \frac{\epsilon_p}{\epsilon_m} \times 100 \quad (3)$$

where ϵ_m is the applied maximum strain, ϵ_u is the fixed strain after unloading and ϵ_p , the permanent strain after induced recovery. The measures were performed with a digital micrometer (measurements were performed in triplicate).

2.2.8 Micro-Computed Tomography (μ -CT)

The shape recovery of the BG-NPs scaffolds inside bone defects produced in the pig femurs bone was evaluated by micro-computerized tomography using a Scanco 20 equipment (Skyscan 1702, Belgium) with penetrative X-rays of 40 keV. The X-ray scans were acquired in high-resolution mode. CT Analyser® was used to visualize the 2D X-ray sections images of the scaffolds. Defects were produced in fresh bones by drilling cylindrical holes with a diameter of 4mm.

3. Results and Discussion

3.1 Bioactivity study

When bioactive bioceramics and glasses, such as Bioglass® are implanted into bone defects, chemical bonding occurs between the surrounding bone tissue and the surface of the implant. Such biomaterials bond to bone via an apatite layer that is formed on their surfaces. Formation of this apatite layer when the material contact with simulated body fluid (SBF) is an *in vitro* bioactivity indicator of the implanted biomaterial¹⁹. Therefore, to analyze the osteoconductive character of the scaffolds, and their potential to be used in bone tissue engineering, the bioactive character of CHT/BG-NPs scaffolds was tested *in vitro* by analyzing the ability to form apatite on their surface after being immersed in SBF.

In this study BG-NPs synthesized by a sol-gel route were used in the preparation of the CHT/BG-NPs composites. The image in Figure IV.1A shows a representative morphology of CHT/BG-NPs scaffold before immersion in SBF. An interconnected porous morphology is observed, with pores of about 50 µm. A higher magnification permits to visualize the BG-NPs embedded in the surface of the porous. The BG-NPs have a spherical appearance with a heterogeneous size of the particles, that could vary in the range 40-100nm. These results confirmed the nanoscale spheroid nature of these particles that spontaneously tend to aggregate in the walls of the pores.

EDS spectra and SEM micrographs of CHT/BG-NPs scaffolds soaked in SBF for 0, 3 and 7 days are presented in Figure IV.1. The bioactive potential of the composite scaffolds produced was confirmed by the development of an apatite layer and the formations of some cauli-flower-like clusters on the surface of the scaffold after immersion in SBF for 3 and 7 days (see SEM image in Figure IV.1B and C). After 7 days of incubation, thin apatite clusters covered almost the entire surface of the scaffolds. Nevertheless some porosity could be seen in the structure despite the apatite deposition.

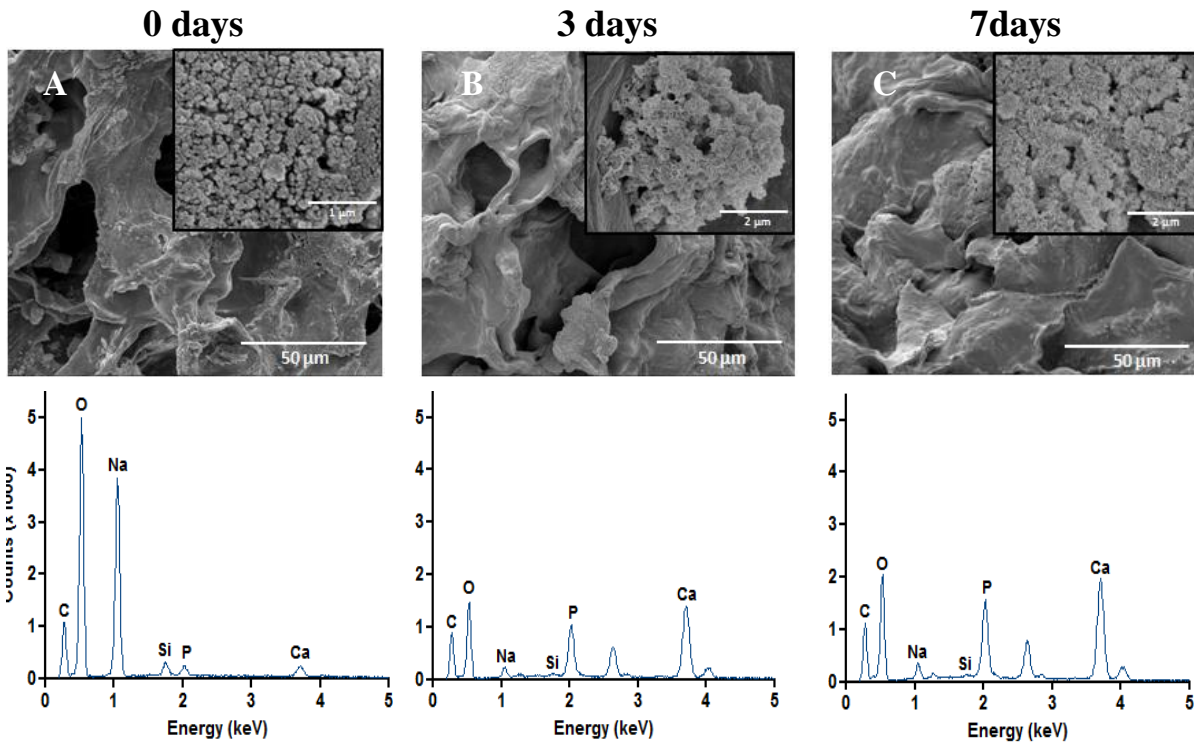


Figure IV.1 - SEM micrographs of CHT/BG-NPs soaked in the SBF solution during 0 (A), 3 (B) and 7 (C) days and the corresponding characterization of the chemical elements using EDS.

EDS analysis of the scaffolds was performed in order to analyze changes in the surface chemical composition related to the mineralization process. The EDS results shows that the concentrations of calcium (Ca) and phosphate (P) gradually increase as the concentration of silicon (Si) decreases due to the dissolution of the BG-NPs, supporting the indication of the development of apatite, being consistent with the SEM observations^{18,20}. A slight relative increase in P and Ca peaks from 3 days to 7 days shows that after 7 days of immersion in SBF the scaffolds present a higher amount of apatite than for 3 days. The increasing of mineral deposits with increased incubation time is related to the longer time available for apatite precipitation.

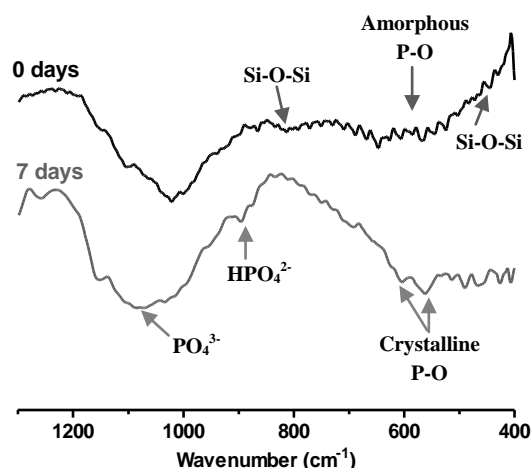


Figure IV.2 - FTIR spectra of the powders scratched from the surface of the patterned membranes after 0 (control) and 7 days of immersion in SBF.

Evolution of apatite formation was also analyzed using FTIR (Figure IV.2). The spectra presented correspond to the apatite powder scratched from the patterned scaffold after 0 and 7 days of immersion in SBF. Before soaking in SBF, the sample exhibited bending and stretching vibrations at 460 and 810 and 1030 cm^{-1} which are assigned to Si-O-Si, consistent with the silica network existing in the BG-NPs²¹. Silicate-related bands are more intense in the control sample, which is in accordance with the previous observations that the Si content decreases after being soaked in SBF.

After 7 days, the samples exhibit a vibration band at 1080 cm^{-1} and a double peak at 607 and 570 cm^{-1} , due to the stretching vibration of phosphate groups¹⁷. After 7 days, the amorphous band in the control sample at around 600 cm^{-1} in SBF evolves into these two peaks of P-O, indicating the hydroxyapatite growth on the surface of the material.

3.2 Swelling of CHT and CHT/BG-NPs scaffolds in water/ethanol mixtures

Swelling test were used to evaluate the absorption capabilities of CHT and CHT/BG-NPs scaffolds in mixtures of a non-solvent (ethanol) and solvent (water). The combined effect of solvent and non-solvent in miscible liquid pairs is expected to be rather useful to control the swelling ratio within polymer networks. Ethanol was used as a non-solvent, aiming at provide control over the scaffolds swelling capability. The

water-uptake capability is an important property of the scaffold to be used as a shape memory device induced by hydration.

As shown in Figure IV.3, the solvent uptake ability of both scaffolds increases with increasing of the water content. Below 50 vol.% such increase is not evident but above such values the swelling starts to increase prominently in both cases. This jump observed above 50 vol.% in the swelling ratio of the scaffolds is a strong indication that this polymer can undergo a phase transition when subject to a change in the solvent composition, at which an abrupt change in the volume is observed. Such event is related to the glass transition that is taking place at this hydration level^{9,10}. At higher water contents a plateau in the swelling curve, is seen, corresponding to a rubber-like behavior of the amorphous component of the chitosan, sustained by the crystalline fraction of the material. The swelling results show that CHT/BG-NPs present higher solvent uptake capability than CHT in all water/ethanol compositions, due to the hydrophilic nature of the BG-NPs fraction. The maximum swelling, reached for 100 vol.% of water, is 179 vol.% for CHT and for CHT/BG-NPs is 358 vol.%.

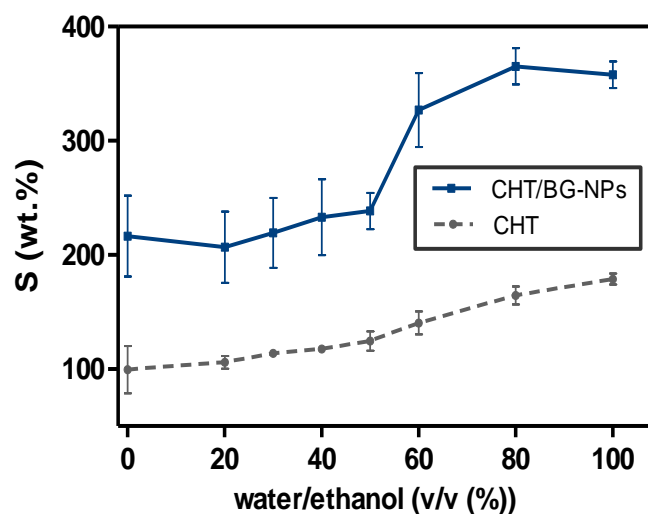


Figure IV.3 - Dependence on the swelling capability of CHT and CHT/BG-NPs scaffolds determined after immersion in water/ethanol mixtures.

3.3 Mechanical Properties

In order to study the CHT/BG-NPs as device with shape memory ability with hydration as a stimulus, using dehydration to fix the temporary shape and hydration to recovery the permanent shape, the mechanical properties and the shape memory

capability of both CHT and CHT/BG-NPs scaffolds were performed for the scaffolds immersed in different mixtures of water/ethanol. The CHT scaffolds were used as a control to analyze how the BG-NPs affect the mechanical properties of the composite.

3.3.1 Young's modulus of the scaffolds at distinct hydration levels

The Young's modulus (E) of the developed scaffolds upon immersion in water/ethanol mixtures was assessed via uniaxial compressive tests, obtained from the slope of the stress-strain curve. Figure IV.4 shows an inverse relationship between E versus water content. For both scaffolds, CHT and CHT/BG-NPs, as the water content was increased, E was observed to systematically decrease. With the decrease of water content, the increasing of E starts for water contents below approximately 50 vol.%. A change at 50 vol% was also mentioned before indicating a glass transition from the glassy to the rubbery state. For water contents above 50% all the samples show a plateau in the elastic modulus, suggesting a rubber-like behavior where the mobile chains in the amorphous regions are sustained by the crystalline domains of chitosan. Water acts as a very good plasticizer, interfering with hydrogen bonds between the chitosan macromolecular chains. The chains acquire greater mobility and the free volume increases, leading to a decrease in the glass transition temperature and the stiffness²². Therefore, increasing plasticizer content resulted in scaffolds with lower E and then more flexible.

The higher value of Young's modulus was observed when the scaffolds were dehydrated being 31.5 kPa for CHT and 55 kPa for CHT/BG-NPs. The mechanical properties are influenced by the incorporation of BG-NPs. The improvement of the Young's modulus is due to the effect of adding a rigid, inorganic particulate phase (BG-NPs) used to reinforce the polymeric matrix. The addition of bioactive glass nanoparticles reinforces the CHT matrix and provides better mechanical properties for the composite scaffold.

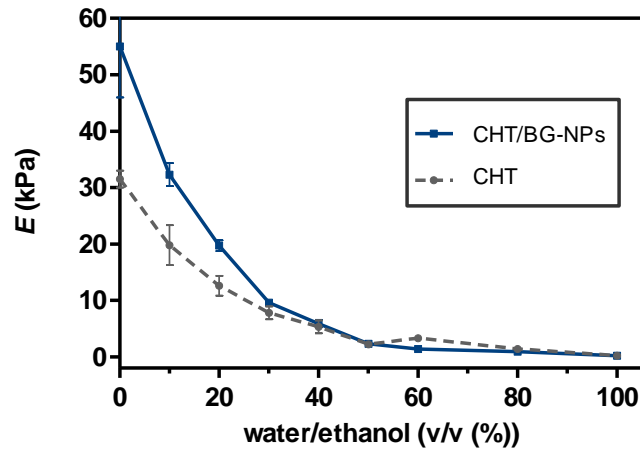


Figure IV.4 - The variation of Young's Modulus with water/ethanol mixtures for CHT and CHT/BG-NPs.

3.3.2 Hydromechanical compressive cyclic

The shape memory effect of CHT and CHT/BG-NPs scaffolds can be represented by hydromechanical cycle. The process across the changing between the permanent and the temporary shape can be divided in 4 steps: loading, dehydration, unloading and recovery.

The cycle starts by hydrating the scaffolds followed by a compression at a constant strain rate, resulting in a continuous stress-strain curve. Afterwards the temporary shape is fixed by dehydrating the scaffold at constant compression ($\epsilon_m=30\%$). Then, the compressive stress is reduced until a stress-free condition is reached. The scaffold is finally hydrated while the compressive stress is kept constant at $\sigma = 0$ kPa. Such process was performed by immersing the scaffolds in water/ethanol mixtures with increasing water content. The permanent shape is recovered, resulting in the strain-water content relationship. The three-dimensional stress-strain-hydration response of both CHT and CHT/BG-NPs scaffolds under uniaxial loading is shown in Figure IV.5.

The stress-strain curves were performed for CHT and CHT/BG-NPs in hydrated conditions by compression tests up to $\epsilon_m = 30\%$ (curve I in Figure IV.5). The scaffolds exhibited a typical response observed in soft cellular materials for relatively low deformations. After loading, ϵ_m is maintained while the samples are dehydrated (stage II in Figure IV.5). When the stress is removed the scaffolds reach the temporary shape (stage III in Figure IV.5).

The strain-hydration curves present in the compressive cycle were obtained by hydration of the dehydrated scaffolds in mixtures of water and ethanol, varying from

pure ethanol to pure water (sequence IV in Figure IV.5). As can be seen, in the hydration process, the strain is recovered significantly above 50% of water content.

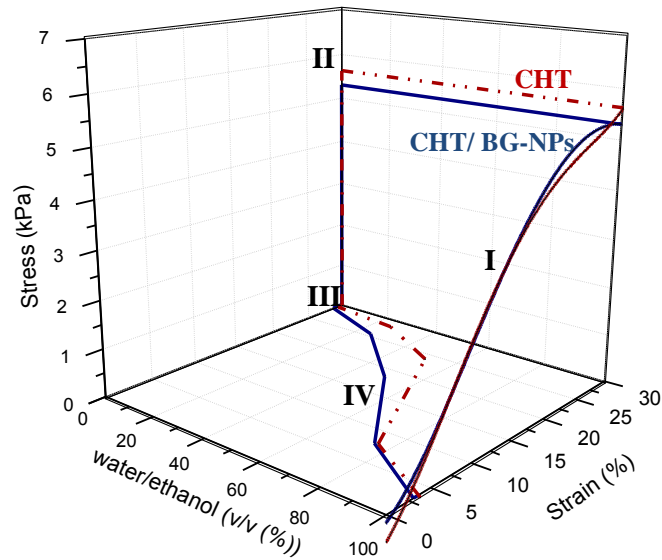


Figure IV.5 - Hydromechanical compressive cycle of CHT and CHT/BG-NPs. I: compression at a constant rate of the hydrated sample; II - dehydration of the sample at a fixed strain; III - release of the stress; IV - hydration in water/ethanol mixtures with increase content in water.

Figure IV.6 shows the variation of strain recovery along hydration for CHT and CHT/BG-NPs scaffolds from a temporary strain (ϵ_m) of 30%. The scaffolds don't exhibit significant strain recovery for water content below 25 vol.%. The strain recovery starts between 25 and 50 vol.% having a drastically increase in the range of 50-75 vol.%. The water has a plasticizing effect on the chitosan increasing the flexibility of the macromolecular chains, leading to a reduction in the transition temperature and resulting in shape recovery. Such results are consistent with the swelling results in Figure IV.3 in which an abrupt change in the volume is observed above 50 vol. % of water content.

The shape fixity R_f and the shape recovery R_r were calculated to quantify the fixation of the temporary and the recovery of the permanent shape of the polymer network. Both CHT and CHT/BG-NPs exhibit good shape memory properties. For a maximum strain of 30% the recovery of the original shape was 87.5% for CHT and 89.9% for CHT/BG-NPs, while the fixation of the deformation shape was 97.2% for CHT and 98.2% for CHT/BG-NPs. CHT/BG-NPs exhibit better shape memory properties than CHT. The addition of Bioglass-nanoparticles reinforces the chitosan matrix and provides bioactive properties for the composite scaffold.

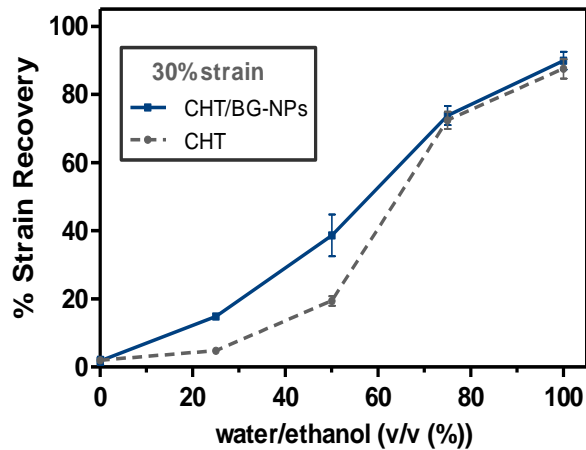


Figure IV.6 - Strain recovery of CHT and CHT/BG-NPs in different mixtures of water/ethanol for $\epsilon_m=30\%$.

As an exemplification of the applicability of the shape memory effect of the scaffolds we placed a previously deformed structure in a bone defect model. A defect was produced in a fresh pig femur with a size between the permanent shape and the temporary shape of the scaffolds. The dehydrated CHT/BG-NPs scaffold in the temporary shape was placed in the empty space and Figure IV.7A shows an image of the system after the introduction of the scaffold and the recovery process shape induced by hydration. We observe that the scaffold accommodate the empty space to filling its geometrical contour. Micro-CT was performed to verify if the recovered scaffold completely fill the bone defect. Figure IV.7B shows that the recovery is guided by the empty space volume and the hydrated scaffold fits perfectly the geometry of the bone defect.

These results strengthen the hypothesis that CHT/BG-NPs have potential as shape-memory bone implant materials for tissue regeneration, in which the scaffolds can be introduced with smaller volumes in bone defect, thus requiring less invasive procedures.

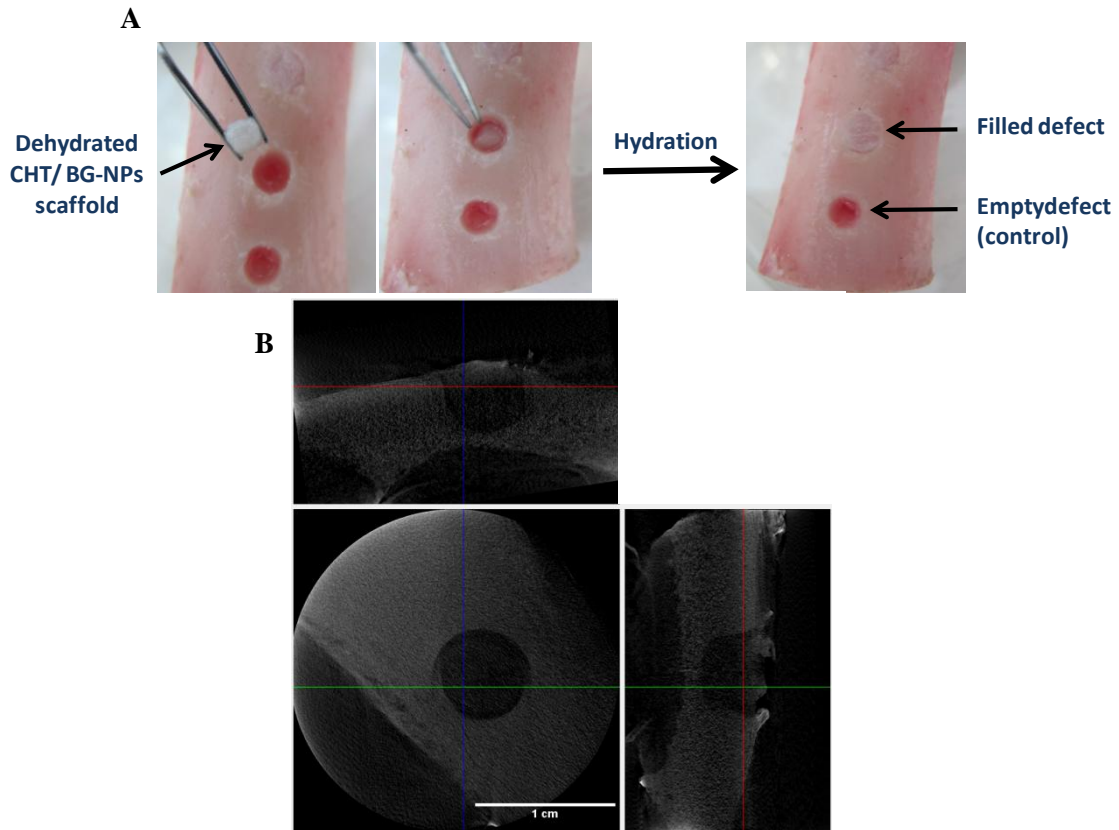


Figure IV.7 - A- Illustration of CHT/BG-NPs recovery in a defect produced in a pig femur bone. B - Representative images of three orthogonal Micro CT slices of a CHT/BG-NPs scaffold after recovery in the bone defect.

4. Conclusion

CHT/BG-NPs composite scaffolds were fabricated and studied for possible application as shape-memory bone implantable materials for tissue regeneration. Upon immersion in SBF the composite scaffolds were able to promote the deposition of an apatite layer, evidencing of an osteoconductive potential. The introduction of BG-NPs in the chitosan matrix increased the stiffness of the scaffolds. Both CHT and CHT/BG-NPs exhibit good shape memory properties. For a maximum strain of 30% the recovery of the original shape was 87.5% for CHT and 89.9% for CHT/BG-NPs, while the fixation of the deformation shape was 97.2% for CHT and 98.2% for CHT/BG-NPs. CHT/BG-NPs exhibit better shape memory properties than CHT. Shape memory capability permits a better fixation and geometrical accommodation of the scaffold in bone defects.

These results suggest that combining chitosan with BG-NPs, we ally the mineralization induced by the BG-NPs with the shape memory capability of the

chitosan biopolymer, producing a nanocomposite with potential applications in bone tissue engineering.

5. Acknowledgments

This work was supported by the Portuguese Foundation for Science and Technology Foundation (FCT) through project PTDC/FIS/115048/2009. We also acknowledge Dr. Ana Rita Duarte for her contribution to the micro-CT analysis.

6. References

- 1 Lendlein, A. *Shape-Memory Polymers*. Vol. 226 (Springer, 2009).
- 2 Liu, Y., Lv, H., Lan, X., Leng, J. & Du, S. Review of electro-active shape-memory polymer composite. *Composites Science and Technology* **69**, 2064-2068 (2009).
- 3 Gall, K. *et al.* Shape memory polymer nanocomposites. *Acta Materialia* **50**, 5115-5126 (2002).
- 4 Leng, J., Lan, X., Liu, Y. & Du, S. Shape-memory polymers and their composites: stimulus methods and applications. *Progress in Materials Science* **56**, 1077-1135 (2011).
- 5 Gunes, I. S. & Jana, S. C. Shape memory polymers and their nanocomposites: a review of science and technology of new multifunctional materials. *Journal of Nanoscience and Nanotechnology* **8**, 1616-1637 (2008).
- 6 Mano, J. *et al.* Natural origin biodegradable systems in tissue engineering and regenerative medicine: present status and some moving trends. *Journal of the Royal Society Interface* **4**, 999-1030 (2007).
- 7 Alves, N. & Mano, J. Chitosan derivatives obtained by chemical modifications for biomedical and environmental applications. *International Journal of Biological Macromolecules* **43**, 401-414 (2008).
- 8 Dash, M., Chiellini, F., Ottenbrite, R. & Chiellini, E. Chitosan—A versatile semi-synthetic polymer in biomedical applications. *Progress in Polymer Science* **36**, 981-1014 (2011).
- 9 Mano, J. F. Viscoelastic properties of chitosan with different hydration degrees as studied by dynamic mechanical analysis. *Macromolecular bioscience* **8**, 69-76 (2008).
- 10 Caridade, S. G., da Silva, R. M., Reis, R. L. & Mano, J. F. Effect of solvent-dependent viscoelastic properties of chitosan membranes on the permeation of 2-phenylethanol. *Carbohydrate Polymers* **75**, 651-659 (2009).
- 11 Kong, L. *et al.* A study on the bioactivity of chitosan/nano-hydroxyapatite composite scaffolds for bone tissue engineering. *European polymer journal* **42**, 3171-3179 (2006).
- 12 Hong, Z., Merino, E. G., Reis, R. L. & Mano, J. F. Novel Rice-shaped Bioactive Ceramic Nanoparticles. *Advanced Engineering Materials* **11**, B25-B29 (2009).
- 13 Rezwani, K., Chen, Q., Blaker, J. & Boccaccini, A. R. Biodegradable and bioactive porous polymer/inorganic composite scaffolds for bone tissue engineering. *Biomaterials* **27**, 3413-3431 (2006).
- 14 Alves, N., Leonor, I., Azevedo, H. S., Reis, R. & Mano, J. Designing biomaterials based on biomineralization of bone. *Journal of Materials Chemistry* **20**, 2911-2921 (2010).

-
- 15 Jell, G. & Stevens, M. Gene activation by bioactive glasses. *Journal of Materials Science: Materials in Medicine* **17**, 997-1002 (2006).
 - 16 Boccaccini, A. R. *et al.* Polymer/bioactive glass nanocomposites for biomedical applications: A review. *Composites Science and Technology* **70**, 1764-1776 (2010).
 - 17 Hong, Z., Reis, R. L. & Mano, J. F. Preparation and in vitro characterization of novel bioactive glass ceramic nanoparticles. *Journal of Biomedical Materials Research Part A* **88**, 304-313 (2009).
 - 18 Luz, G. M. & Mano, J. F. Preparation and characterization of bioactive glass nanoparticles prepared by sol-gel for biomedical applications. *Nanotechnology* **22**, 494014 (2011).
 - 19 Kokubo, T. & Takadama, H. How useful is SBF in predicting in vivo bone bioactivity? *Biomaterials* **27**, 2907-2915 (2006).
 - 20 Hong, Z., Reis, R. L. & Mano, J. F. Preparation and in vitro characterization of scaffolds of poly (L-lactic acid) containing bioactive glass ceramic nanoparticles. *Acta Biomaterialia* **4**, 1297-1306 (2008).
 - 21 Ma, J., Chen, C., Wang, D., Meng, X. & Shi, J. In vitro degradability and bioactivity of mesoporous CaO-MgO-P₂O₅-SiO₂ glasses synthesized by sol-gel method. *Journal of sol-gel science and technology* **54**, 69-76 (2010).
 - 22 Yang, B., Huang, W., Li, C. & Li, L. Effects of moisture on the thermomechanical properties of a polyurethane shape memory polymer. *Polymer* **47**, 1348-1356 (2006).

Chapter V. - General Conclusions and Future Perspectives

General Conclusions and Future Perspectives

The shape memory potential of chitosan scaffolds was present and characterized in this work. Non-crosslinked and crosslinked CHT scaffolds showed shape memory effect under hydration as stimuli, with shape fixity by dehydration and shape recovery by hydration. The swelling in water/ethanol mixtures showed that both scaffolds have good water uptake capability, which may be a result of the interconnected porous structure revealed. Moreover, they presented a jumpwise change in the volume of the scaffolds around 40 vol.% of water, which was a strong indication that the swelling can determinate the mechanical behavior of scaffolds.

By DMA analysis it was possible to verify a glass transition for both scaffolds induced by hydration. CHT0 present a glass transtion of 32.3 vol.% of water in water/ethanol mixtures and CHT1 at 40 vol.%. The Young's modulus (E) was assessed via compressive tests and was observed an inverse relationship between E and water content. The E starts to increase in the vicinity of the glass transition, for water contents below approximately 40 vol.%. For water contents above 40 vol.%, all the samples showed a plateau in the Young's modulus, suggesting a rubber like structure where the mobile chains in the amorphous regions are sustained by crystalline or crosslinked domains.

The recovery along time for different maximum strain for CHT0 showed a rapid recovery that occurs essentially in the first 5 minutes. The recovery dependence with hydration was also evaluated for both scaffolds. The scaffolds exhibit a drastically recovery for water content above 50 vol.% which are according with the jump observed in the swelling results and with the peak observed in DMA analyses. The recovery decreased with increasing of maximum strain and CHT1 presented better mechanical properties and better recoverability than CHT0. Results showed that chitosan possess shape memory properties, characterized by a fixity ratio above 97.2% for CHT0 and above 99.2% for CHT1 and a recovery ratio above 70.5% for CHT0 and 98.5% for CHT1. Aftwards, *in vitro* drug delivery studies were also performed to demonstrate that such devices can be also loaded with molecules. The results showed that the CHT1

release more amount of molecule than CHT1, but both scaffolds showed that this system can be used as controlled delivery system.

In the following chapter the chitosan were combined with bioactive glass nanoparticles for possible application as a shape-memory implant material for bone regeneration. The EDS, FTIR and SEM results from *in vitro* bioactivity studies showed a development of an apatite layer on the surface of the scaffolds also proved by a decreasing of Si content and an increasing of Ca and P content after 7 days. The mechanical properties of BG-NPs scaffolds in terms of shape memory showed the same behavior of CHT and CHT1 with a jumpise in the swelling behavior for water contents around 50 vol% and a decreasing of E with increasing of water content followed by a plateau above 50 vol.%, which is a response from a glass transition, also observed in the previous chapter. CHT/BG-NPs scaffolds showed a shape recovery of 87.5% and a shape fixity of 98.2%. CHT/BG-NPs present better mechanical properties that CHT, as a result from the incorporation of BG-NPs.

The properties and behavior of the scaffolds developed showed that they are candidates for applications in minimally invasive surgery for tissue regeneration or for drug delivery. Moreover, the incorporation of BG-NPs allows potential applications in bone regeneration.

After this study, and based on the good shape memory properties that all the scaffolds developed showed, the next step would be the establishment of *in vivo* tests, using adequate animal models to evaluate the performance of these scaffolds inside of a living body. Moreover, the potential of the scaffolds as a drug delivery system should be tested for different types of drugs and molecules addressed for different applications.

The shape memory behavior observed in CHT and based on the fact that CHT is a material with great versatility to be processed in different structures can be used to produce different types of chitosan-based devices to be used as a shape memory implant for different approaches. To overcome mechanical and malleable disadvantages of CHT, composites with others polymers could be also tested.
